

BRL CR 38

BRL

AD

CONTRACT REPORT NO. 38

3SR-348

AD 725732

EFFECTS OF PROJECTILE SHAPE ON THIN PLATE PERFORATION AT NORMAL INCIDENCE

Prepared by

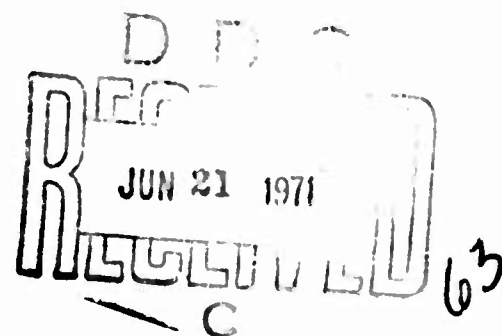
Systems, Science and Software
La Jolla, California

May 1971

This document has been approved for public release and sale;
its distribution is unlimited.

Reproduced by
NATIONAL TECHNICAL
INFORMATION SERVICE
Springfield, Va. 22151

U.S. ARMY ABERDEEN RESEARCH AND DEVELOPMENT CENTER
BALLISTIC RESEARCH LABORATORIES
ABERDEEN PROVING GROUND, MARYLAND



Destroy this report when it is no longer needed.
Do not return it to the originator.

| | | |
|---------------------------------|---------------|--|
| ACCESSION for | | |
| CFSTI | WHITE SECTION | <input checked="checked" type="checkbox"/> |
| DDC | BUFF SECTION | <input type="checkbox"/> |
| UNANNOUNCED | | <input type="checkbox"/> |
| JUSTIFICATION | | |
| BY | | |
| DISTRIBUTION/AVAILABILITY CODES | | |
| DIST. | AVAIL. | SPECIAL |
| A | | |

The findings in this report are not to be construed as
an official Department of the Army position, unless
so designated by other authorized documents.

Unclassified

Security Classification

DOCUMENT CONTROL DATA - R & D

(Security classification of title, body of abstract and indexing annotation must be entered when the overall report is classified)

| | | | |
|--|--|---|------------------------------|
| 1. ORIGINATING ACTIVITY (Corporate author) Systems, Science and Software P.O. Box 1620 La Jolla, California 92123 | | 2a. REPORT SECURITY CLASSIFICATION Unclassified | |
| | | 2b. GROUP | |
| 3. REPORT TITLE Effects of Projectile Shape on Thin Plate Perforation at Normal Incidence | | | |
| 4. DESCRIPTIVE NOTE (Type of report and inclusive dates) | | | |
| 5. AUTHOR(S) (First name, middle initial, last name) R. T. Sedgwick J. M. Walsh | | | |
| 6. REPORT DATE May 1971 | | 7a. TOTAL NO. OF PAGES 59 | 7b. NO. OF REFS 10 |
| 8a. CONTRACT OR GRANT NO. DAAG 07-68-C-0931 | | 8b. ORIGINATOR'S REPORT NUMBER(S) 3SR-348 | |
| 8c. PROJECT NO. RDT&E 1T650212D620 | | 8d. OTHER REPORT NO(S) (Any other numbers that may be assigned this report) BRL Contract Report No. 38 | |
| 10. DISTRIBUTION STATEMENT This document has been approved for public release and sale; its distribution is unlimited. | | | |
| 11. SUPPLEMENTARY NOTES <i>Superseded</i> AD-882673 | | 12. SPONSORING MILITARY ACTIVITY USA Aberdeen Research & Development Center Ballistic Research Laboratories Aberdeen Proving Ground, Maryland 21005 | |
| 13. ABSTRACT Analytical, numerical and experimental results are compared in a systematic investigation of the effects of projectile shaped on thin plate perforation. The analysis of five low velocity impact involving optimal-, ogival-, Russian-, conical- and cylindrical-head projectile comprise the study. A three-way comparison of simple perforation theory predictions, HELP numerical solutions and available experimental data is made for the five problems. The HELP solutions are in excellent agreement with the experimental data. Although the simple perforation formulas are sensitive to projectile shape, they do not provide adequate residual energy predictions. Further numerical studies of this type should provide additional insight into the penetration process and eventually lead to improved perforation formulas. | | | |

DD FORM 1473

REPLACES DD FORM 1473, 1 JAN 64, WHICH IS OBSOLETE FOR ARMY USE.

Unclassified

Security Classification

| 14. KEY WORDS | LINK A | | LINK B | | LINK C | |
|---|--------|----|--------|----|--------|----|
| | ROLE | WT | ROLE | WT | ROLE | WT |
| Impact Thin Plates Projectile Shape Effects Petalling Failure Numerical Solutions | | | | | | |

BALLISTIC RESEARCH LABORATORIES

CONTRACT REPORT NO. 38

3SR-348

MAY 1971

**EFFECTS OF PROJECTILE SHAPE ON THIN PLATE
PERFORATION AT NORMAL INCIDENCE**

FINAL REPORT

**R. T. Sedgwick
J. M. Walsh**

Prepared By:

**SYSTEMS, SCIENCE AND SOFTWARE
La Jolla, California**

**This document has been approved for public release and sale;
its distribution is unlimited.**

**Contract No. DAAG 07-68-C-0931
and
RDT&E Project No. 1T650212D620**

ABERDEEN PROVING GROUND, MARYLAND

BALLISTIC RESEARCH LABORATORIES

CONTRACT REPORT NO. 38

3SR-348

**RTSedgwick/JMWalsh
Aberdeen Proving Ground, Md.
May 1971**

**EFFECTS OF PROJECTILE SHAPE ON THIN PLATE
PERFORATION AT NORMAL INCIDENCE**

ABSTRACT

Analytical, numerical and experimental results are compared in a systematic investigation of the effects of projectile shape on thin plate perforation. The analysis of five low velocity impacts involving optimal-, ogival-, Russian-, conical- and cylindrical-head projectiles comprise the study. A three-way comparison of simple perforation theory predictions, HELP numerical solutions and available experimental data is made for the five problems.

The HELP solutions are in excellent agreement with the experimental data. Although the simple perforation formulas are sensitive to projectile shape, they do not provide adequate residual energy predictions. Further numerical studies of this type should provide additional insight into the penetration process and eventually lead to improved perforation formulas.

CONTENTS

| | |
|--|----|
| List of Symbols | ii |
| I. INTRODUCTION | 1 |
| II. SIMPLE PERFORATION FORMULAS | 4 |
| 2.1 Thomson Model | 5 |
| 2.2 Zaid and Paul Model | 7 |
| 2.3 Nishiwaki Model | 9 |
| 2.4 Recht and Ipson Model | 9 |
| 2.5 Heyda Model | 12 |
| III. COMPARISON OF FORMULAS WITH EXPERIMENT | 14 |
| IV. NUMERICAL SOLUTIONS | 17 |
| 4.1 Numerical Techniques | 17 |
| 4.2 Material Model | 20 |
| 4.3 Numerical Results | 22 |
| V. DISCUSSION OF RESULTS | 36 |
| VI. CONCLUSIONS | 42 |
| References | 43 |
| Appendix: Russian Projectile-Target Configurations at Various Times | 44 |

LIST OF SYMBOLS

| | | |
|--|---|---|
| A | - | Constant used in the Tillotson equation of state for a given material |
| A' | - | Projectile-plate contact area |
| $\left. \begin{matrix} a \\ \alpha \\ B \\ b \\ \beta \end{matrix} \right\}$ | - | Constant used in the Tillotson equation of state for a given material |
| C_p | - | Hydrodynamic sound speed in projectile material |
| C_t | - | Hydrodynamic sound speed in target material |
| D | - | Diameter of plug |
| de'_{ij} | - | Deviatoric strain increments |
| dS'_{ij} | - | Deviatoric stress increments |
| Δt | - | Time step employed in HELP solution |
| η | - | ρ/ρ_0 |
| G | - | Shear modulus |
| h_0 | - | Plate thickness |
| I | - | Specific internal energy |
| I_m | - | Specific internal energy necessary for melting a particular material |
| $\left. \begin{matrix} I_0 \\ I_s \\ I'_s \end{matrix} \right\}$ | - | Specific internal energy constants used in the Tillotson equation of state for a given material |
| i | - | Number associated with a particular vertical grid line in HELP ($i = 0$ to i_{MAX}) |
| i_{MAX} | - | Maximum number of vertical grid lines employed |
| j | - | Number associated with a particular horizontal grid line in HELP ($j = 0$ to j_{MAX}) |
| j_{MAX} | - | Maximum number of horizontal grid lines employed |

| | |
|---|--|
| $\left. \begin{matrix} K_0 \\ K_1 \\ K_2 \end{matrix} \right\}$ | Constants for a given material which determine the variation of yield strength with density |
| L | Axial length of nose of pointed projectiles (Total projectile length for the case of a cylinder) |
| l | Cylindrical projectile length at any time after impact |
| M_p | Mass of projectile |
| M_t | Axial component of plate momentum |
| μ | $\rho/\rho_0 - 1$ |
| Ω | Ratio of target to projectile mass density |
| P_0 | Empirically determined static pressure component |
| p | Pressure |
| p_c | Pressure obtained using condensed form of Tillotson equation of state |
| p_E | Pressure obtained using expanded form of Tillotson equation of state |
| R | Maximum projectile radius |
| r_0 | Initial radial distance of any mass element which later forms part of the petal |
| ρ | Mass density |
| ρ_0 | Initial mass density for a particular material |
| ρ_p | Mass density of projectile material |
| ρ_T | Mass density of target material |
| σ_y | Plate material yield strength |
| t | Time |
| θ | Half angle for conical nosed projectile |
| V | Projectile velocity during penetration |

| | |
|----------|---|
| V_o | = Projectile velocity at instant of impact |
| V_r | = Projectile residual velocity |
| V_{xn} | = Minimum perforation velocity |
| v | = $1/\rho$ |
| v_o | = $1/\rho_o$ |
| W | = Reduction in projectile kinetic energy |
| x | = x-coordinate of a point on the projectile surface |
| x' | = Distance between tip of projectile and original plate position |
| ξ | = Axial distance between a mass element of the petal and its original position (x) in the plate |
| Y | = Yield strength in shear (varies with density and energy) |
| y | = Projectile nose radius as a function of distance from tip of projectile |
| y_o | = Constant yield strength in shear (plate material) |

I. INTRODUCTION

A few basic considerations suffice to indicate the motivation for the present numerical analysis of projectile shape effects. The efficiency with which a kinetic energy penetrator is able to defeat a particular target is dependent on the configurational and material parameters as well as the mode of plate failure. Existing perforation formulas cannot accurately predict this dependency. Furthermore, the application of these formulas requires that the plate failure mode be assumed in advance. Numerical techniques, however, can be used as a tool to investigate the complicated relationships between material and configurational parameters, material flow history, failure criteria and plate failure mode. Such techniques should therefore be useful in predicting penetration efficiency and provide useful information to designers of both weapons and armor as well as to vulnerability analysts.

Penetration efficiency is a difficult parameter to define in general; however, for the case of thin plate perforation, it can be defined as the ratio of residual projectile kinetic energy to initial energy. Even with such a precise definition, penetration efficiency is difficult to calculate analytically since it requires a perforation formula which accurately predicts the residual projectile velocity and which is extremely sensitive to the configurational and material parameters which define a particular impact. Furthermore, since failure modes also depend on impact parameters, a particular thin plate perforation formula can at best be expected to provide good predictions only over a narrow range of parameters. For example, an increase in projectile hardness should increase penetration efficiency; however, if the impact occurs in a regime in which projectile break-up or shattering occurs, penetration efficiency decreases. Another example, and one that will be discussed in the following sections of this report in more detail, involves

the effect of projectile shape. Thin plate failure modes can vary from petalling to plugging as the projectile nose is varied from an extremely pointed to an extremely blunt shape. Combined petalling and plugging modes can occur for intermediate shapes. Since projectile shape is an important parameter to which thin plate penetration efficiency is more sensitive than can be demonstrated by existing perforation formulas, and since it represents a parameter which when varied encompasses more than one plate failure mode, it has been chosen as the subject of the numerical impact investigation reported here.

In Section II various existing thin plate perforation theories are presented. In Section III some recent work by T. E. Fields⁽¹⁾ concerning the comparison of some of the perforation formula predictions with experimental data for various projectile shapes is discussed. The inadequacy of certain of these formulas to predict experimentally observed residual velocities becomes quite apparent. Numerical solutions to five problems chosen to reproduce selected impacts from Fields' experimental matrix⁽¹⁾ are presented in Section IV. The projectile shapes, which will be defined later, are referred to as optimal-, ogival-, Russian-, cylindrical- and conical-head projectiles. The HELP computer code was employed in these solutions. The numerical techniques are briefly described and the material model employed, including the equation of state, deviatoric constitutive relation, yield condition and failure criterion is discussed. The HELP solution to the Russian projectile impact is presented in detail while only selected numerical data from the solutions of the other four problems are included. In Section V the numerical results are discussed and compared with both the predictions from the elementary perforation formulas and the experimental observations.

Finally, Sections VI and VII respectively present the conclusions of the current study (performed under the technical direction of Dr. R. T. Sedgwick) and outline suggestions for additional related research.

This report is the third under the current contract. The first⁽²⁾ applies the HELP code to two specific test problems. The problems were specified to provide a basis of comparison of the HELP approach with Lagrangian methods. The second report⁽³⁾ is a complete documentation and listing of the HELP code.

We believe that the results reported here are very encouraging and point to the desirability of additional applications of the HELP code to armor penetration studies.

II. SIMPLE PERFORATION FORMULAS

A penetration formula can be defined as an expression, theoretically or empirically derived, relating the configurational and material properties which characterize a particular impact situation to those of the residual state. For thick target impacts, where the projectile is defeated, it is customary to describe the residual state by a single parameter, penetration depth (the state of the defeated projectile is usually not of interest). For thin plate perforation, the residual state should include the kinetic energy, velocity, mass and shape of all projectile and target fragments as well as the final target hole size. In the interest of simplicity, however, most thin plate theories are restricted to describing the residual state by the kinetic energy of the major residual particles, only. This simplification is usually arrived at by assuming rigid projectile penetration in conjunction with an a priori choice of hole size and plate failure mode.

A brief summary of low impact velocity penetration mechanics is given in Ref. 4. In the following paragraphs, existing thin plate perforation formulas pertinent to impact situations of interest in the current study are presented. Since the derivations of these formulas are well documented elsewhere⁽⁴⁻⁹⁾ only brief discussions of their nature and applicability as well as the physical assumptions involved in their development are presented with each perforation formula.

2.1 THOMSON MODEL

The perforation formula proposed by Thomson⁽⁵⁾ is based on the assumption that the reduction in projectile kinetic energy is a result of the work done by the projectile in both plastic deformation and radial motion of the displaced target material. The projectile is assumed to be rigid and the target material is assumed to behave in a rigid-perfectly plastic manner. In addition, the radial and axial stresses are assumed small, relative to circumferential stresses. Finally, it is assumed that the hole size equals the maximum projectile radius, that plastic deformation occurs without a change in volume, and that energy loss due to frictional forces at the projectile-target interface are negligible.

For the variables defined in Fig. 1, the reduction in projectile kinetic energy, according to Thomson's theory, can be expressed as

$$W = \frac{\pi R^2 h_0 \sigma_y}{2} + \pi \rho_t h_0 V^2 \left[\int_0^R y^2 \frac{d^2 y}{dx^2} dy + 2 \int_0^R y \left(\frac{dy}{dx} \right)^2 dy \right] \quad (1)$$

where σ_y and ρ_t are the target yield strength and mass density respectively and V is the velocity of penetration which, for simplicity, is assumed to be constant and equated to the impact velocity, V_0 . The expression involving residual velocity, V_r , is obtainable from the energy balance

$$W = \frac{1}{2} M_p V_0^2 - \frac{1}{2} M_p V_r^2 \quad (2)$$

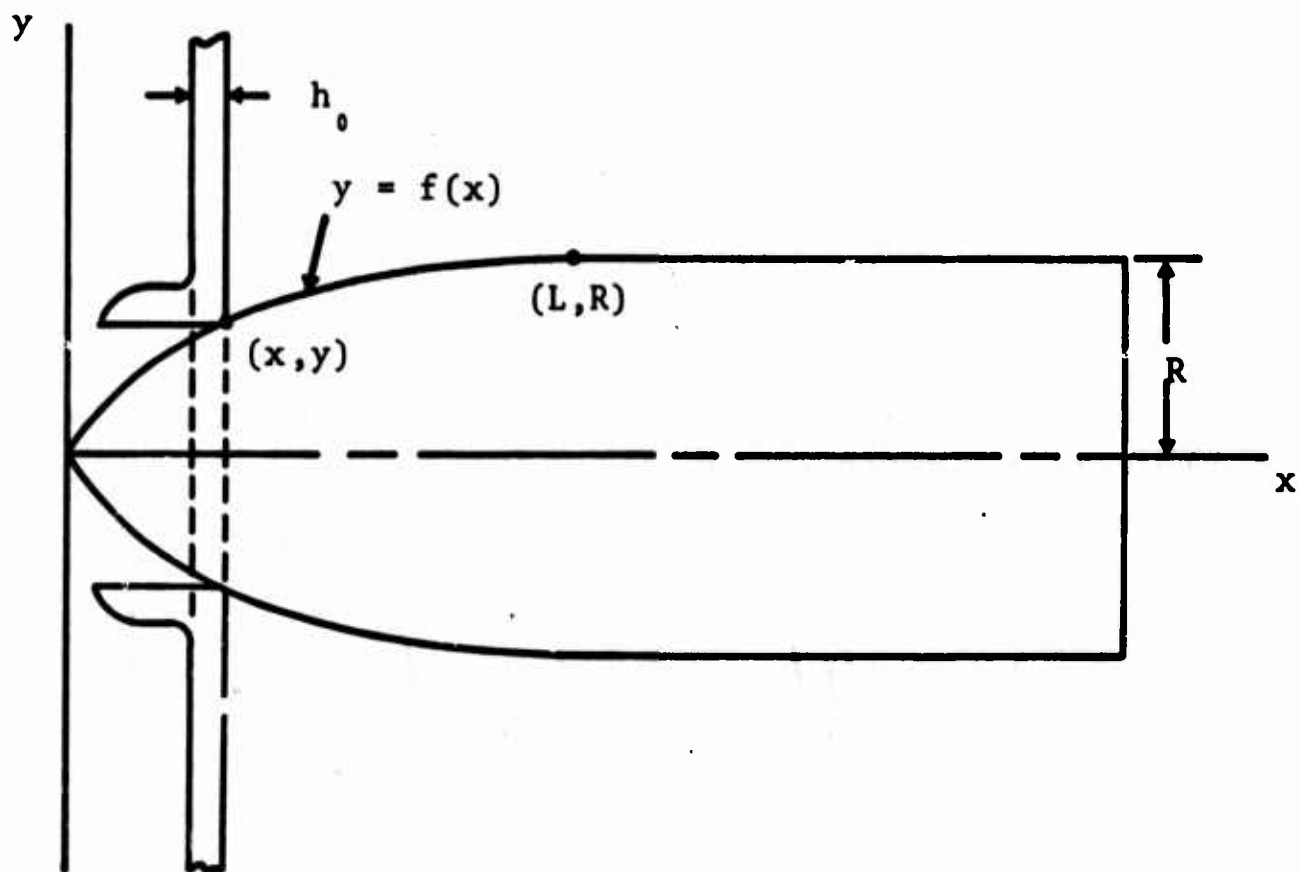


Fig. 1--Projectile target configuration for describing the geometric variables and parameters employed by the Thomson formula. The coordinate system is attached to the projectile.

and becomes

$$V_r^2 = V^2 \left\{ 1 - \frac{2\pi\rho h_0}{M_p} \left[\int_0^R y^2 \frac{d^2 y}{dx^2} dy + 2 \int_0^R y \left(\frac{dy}{dx} \right)^2 dy \right] \right\} - \frac{\pi R^2 h_0 \sigma_y}{M_p} \quad (3)$$

where M_p is the projectile mass.

2.2 ZAID AND PAUL MODEL

Zaid and Paul⁽⁶⁾ in their model make use of conservation of axial momentum during rigid projectile perforation of a thin plate assumed to fail by petalling. Figure 2 illustrates the geometrical parameters and variables employed. Conservation of axial momentum is given by

$$M_p V_0 = M_p V + M_t(x) \quad (4)$$

where V is the instantaneous projectile velocity and $M_t(x)$ is the axial component of plate momentum. For pointed projectiles the total axial momentum imparted to the plate, M_t , can be expressed as

$$M_t = 2\pi\rho h_0 \int_0^R V r_0 \frac{\partial \xi(r_0, x)}{\partial x} dr_0 \quad (5)$$

The equation for projectile velocity loss then becomes

$$V_0 - V_r = \frac{2\pi\rho h_0 V_0}{M_p} \int_0^R r_0 \frac{\partial \xi(r_0, x)}{\partial x} dr_0 \quad (6)$$

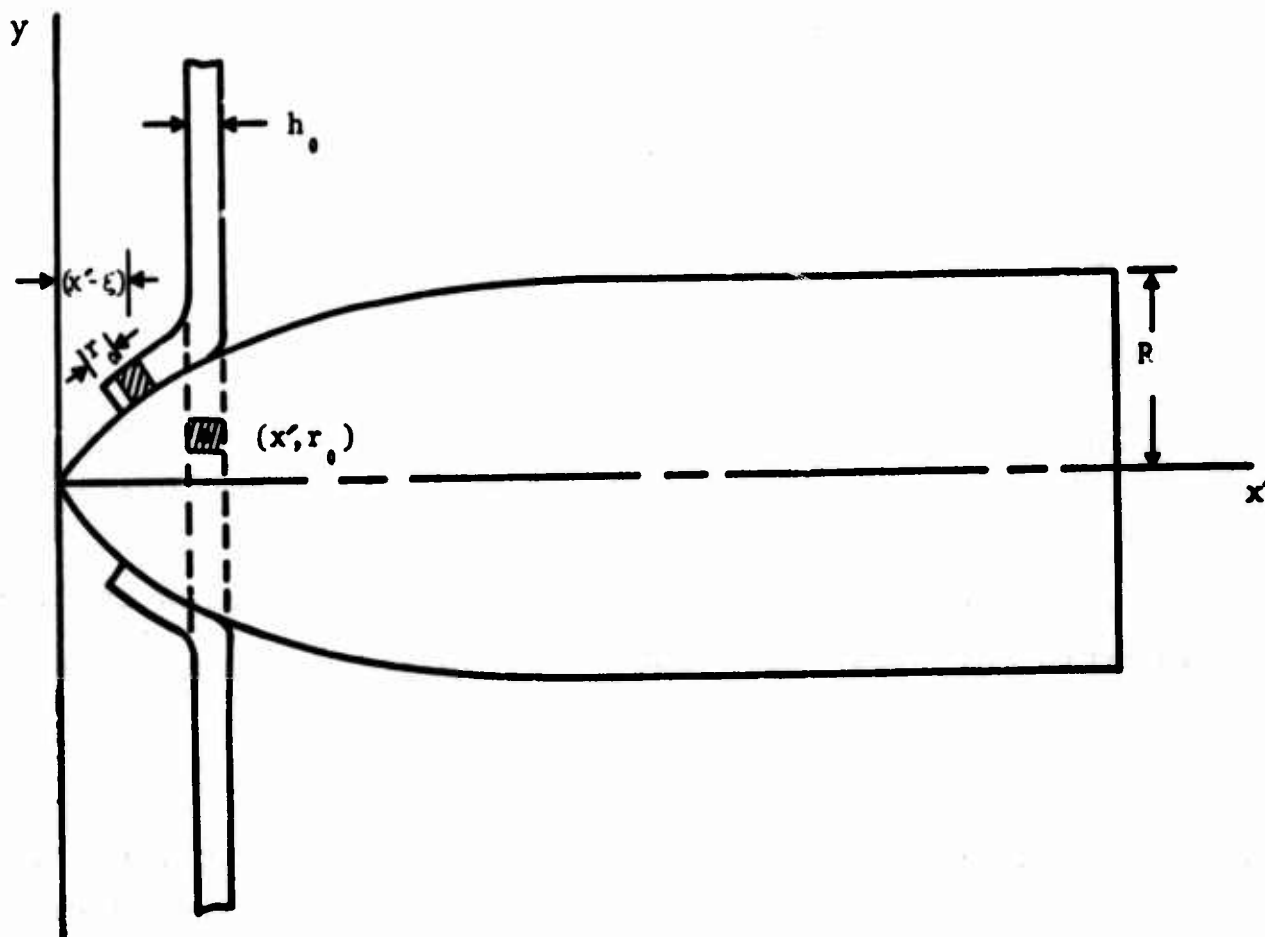


Fig. 2--Projectile-target configuration for describing the geometric variables and parameters employed by the Zaid and Paul formula. The coordinate system is attached to the projectile.

where the instantaneous velocity, V , of Eq. (5) has been approximated by the initial impact velocity, V_0 .

2.3 NISHIWAKI MODEL

The perforation formula developed by Nishiwaki⁽⁷⁾ is arrived at by writing the equation of motion of the projectile acted upon by plate forces due to a static and dynamic pressure as well as frictional forces. For the conical head projectile shown in Fig. 3, the projectile equation of motion, assuming no frictional forces, can be written as

$$M_p \frac{dV}{dt} = - \int_{A'} (P_0 + \rho V^2 \sin^2 \theta) \sin \theta dA' \quad (7)$$

where A' is the projectile-plate contact area and P_0 is an empirically determined static pressure component. The expression for the residual velocity for the conical impact case of Fig. 3 can be obtained by integrating Eq. (7) and is given by Fields⁽¹⁾ as

$$V_r^2 = \left(V^2 + \frac{P_0}{\rho \sin^2 \theta} \right) e^{-\frac{2\pi \rho R^2 h \sin^2 \theta}{M_p}} - \frac{P_0}{\rho \sin^2 \theta} \quad (8)$$

2.4 RECHT AND IPSON MODEL

Recht and Ipson⁽⁸⁾ assume a plugging failure mode and use conservation of momentum and energy to express the reduction in projectile velocity due to both the acceleration of the plug mass and shear resistance at the plug periphery. In terms of the geometrical impact parameters of Fig. 4, the

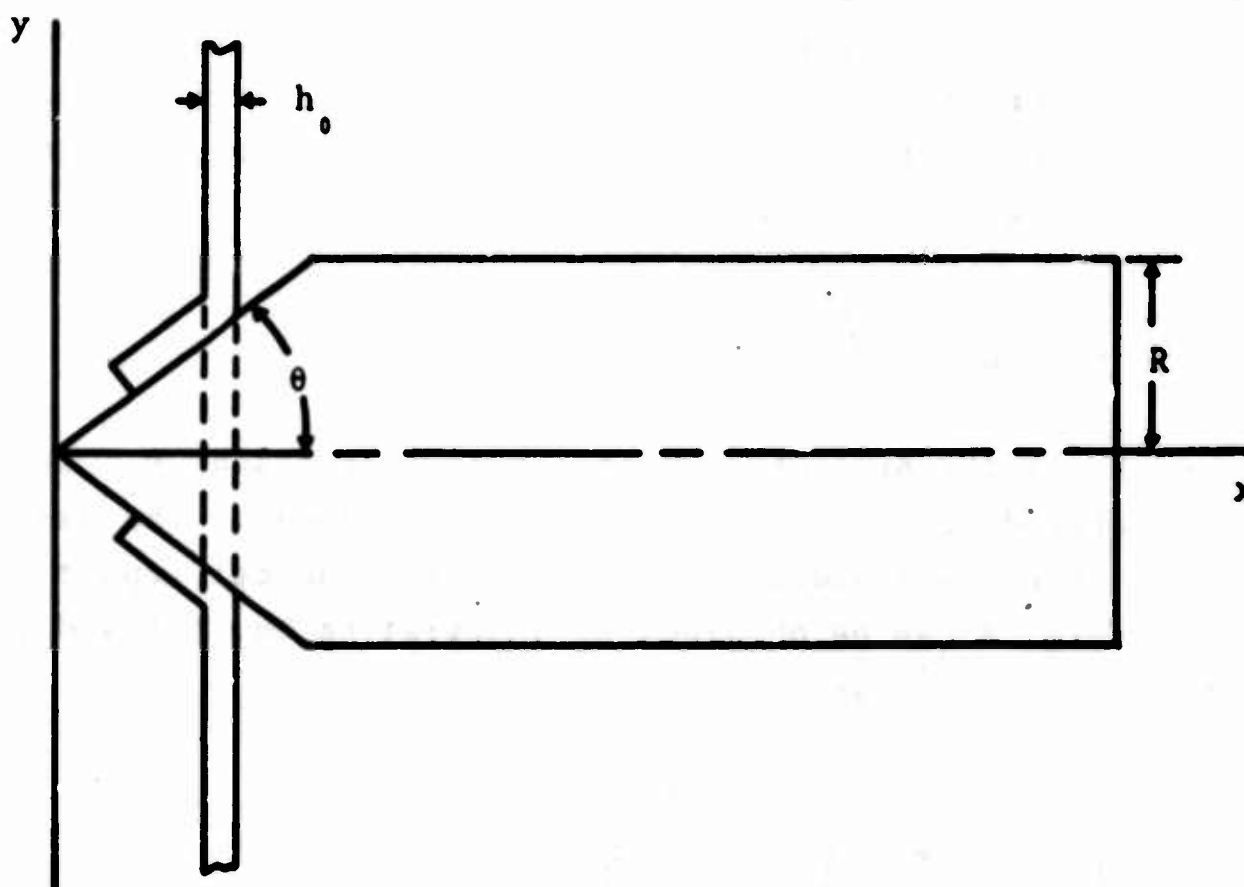


Fig. 3--Projectile-target configuration for describing the geometric variables and parameters employed by the Nishiwaki formula for the case of a conical projectile.

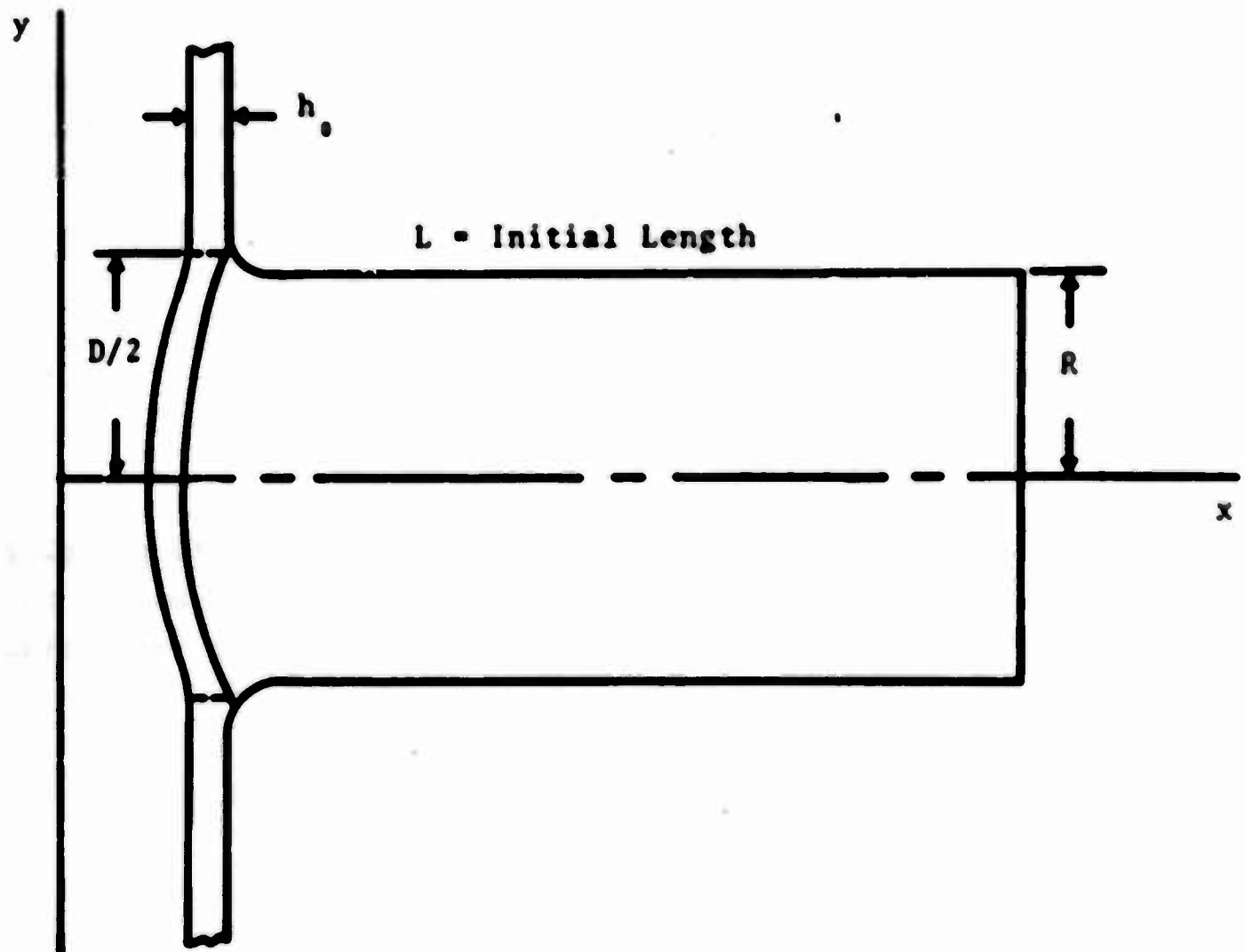


Fig. 4--Projectile-target configuration for describing the geometric parameters employed by the Recht and Ipsen formula for the case of a cylindrical projectile.

expression for residual velocity is

$$V_r = \left[\frac{1}{1 + \Omega \left(\frac{D}{2R} \right)^2 \frac{h}{L}} \right] (V_i^2 - V_{xn}^2)^{1/2} \quad (9)$$

where Ω is the ratio of target to projectile density and V_{xn} is the minimum perforation velocity. Inherent in the development of Eq. (9) is the assumption that the average dynamic shear stress acting on the plug periphery remains constant. It should also be mentioned that the value of V_{xn} must be determined experimentally and an assumption regarding the plug diameter must be made.

2.5 HEYDA MODEL

Heyda⁽⁹⁾ has recently developed a thin plate plugging model which reduces to the theory of Recht and Ipsen for the case of like material impact. Heyda's expression for residual velocity can be written as

$$V_r = \frac{1}{1 + \left(\frac{2}{\frac{c_t}{c_p} + \frac{\rho_p}{\rho_t}} \right) \frac{h}{L}} (V_i^2 - V_{xn}^2)^{1/2} \quad (10)$$

where the subscripts t and p refer to the target and projectile material respectively and c is the hydrodynamic sound speed. Heyda also gives an expression for the minimum perforation velocity, V_{xn} , as

$$V_{xn} = \left\{ \frac{2\gamma h^2}{\rho_p R \ln \left[1 - \frac{4kh}{\rho_p L c_t} \right]} \right\}^{1/2} \quad (11)$$

where

$$n = \frac{2\rho_p c_p}{\rho_t c_t + \rho_p c_p},$$

$$K = \left(\frac{\rho_t c_t}{2} \right) n$$

and l can be taken as the length of the projectile at the time the initial pressure wave is attenuated by the rear free surface rarefaction.

III. COMPARISON OF FORMULAS WITH EXPERIMENT

The following comparison of perforation formula predictions with experimental results is based on the work of T. E. Fields.⁽¹⁾ Fields investigated experimentally the effect of projectile shape on thin target perforation. Five different shapes were analyzed in this study and are referred to here as ogival-, optimal-, Russian-, conical-, and cylindrical-head projectiles. The relative shapes are shown in Fig. 5. The nominal impact velocity for the set of experiments was approximately 5×10^4 cm/sec. The projectile masses were all about 20 g and both steel and aluminum targets were impacted.

Three thicknesses of aluminum plates, namely 0.159, 0.317, and 0.476 cm, were impacted while only one thickness, 0.317 cm, was chosen for the steel plate impacts. Fields compared his experimental results with the predictions of the perforation formulas of Thomson and Nishiwaki. A sample comparison for each projectile shape is given in Table I where it is clearly evident that agreement is less than acceptable. The bracketed values in Table I were calculated by A. J. Good. The remainder of the table is taken from Ref. 1. It was the inability of the perforation formulas to predict the observed residual velocities that lead to the numerical projectile shape effects study discussed in Section IV. The lack of agreement is not surprising in view of the many over-simplifying assumptions required in the development of a simple perforation formula.

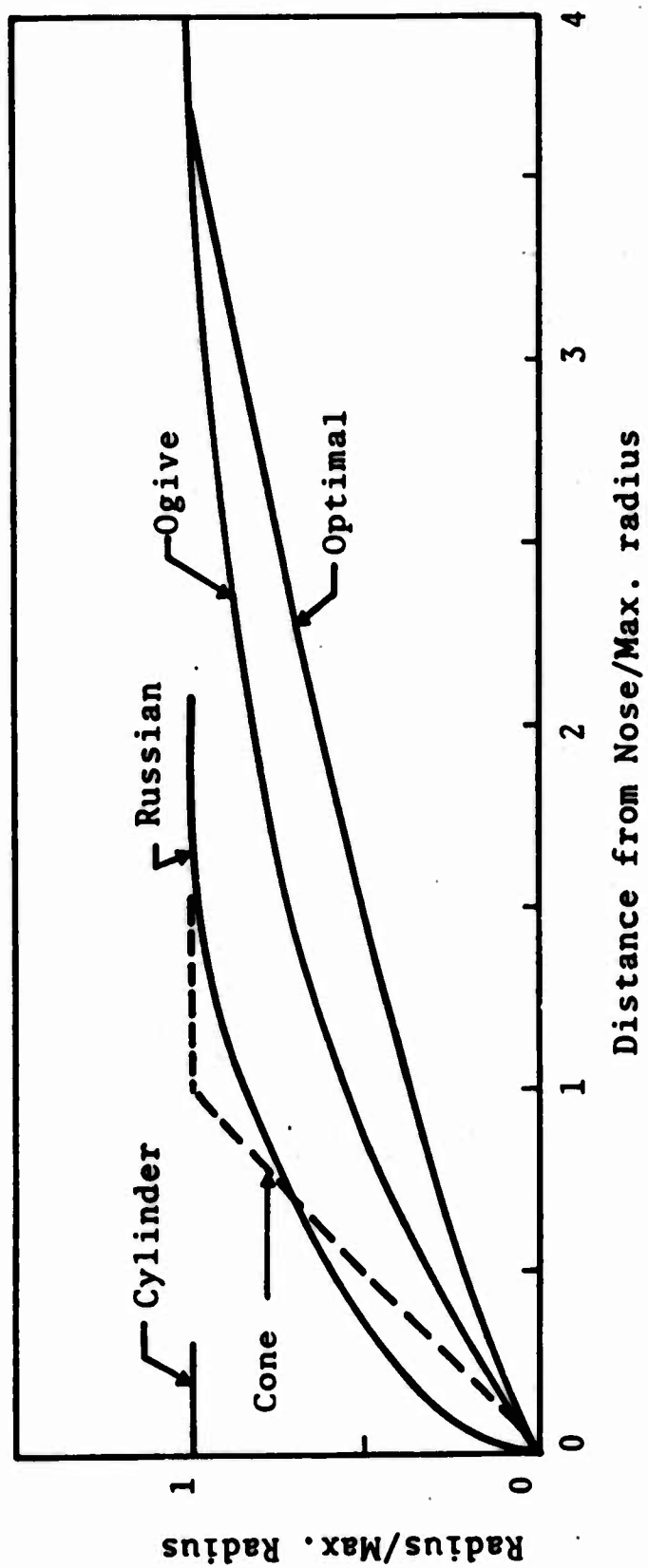


Fig. 5--Relative projectile shapes. This figure is due to T. E. Fields. (1)

TABLE I
SAMPLE COMPARISONS BETWEEN PREDICTED (PERFORATION FORMULAE)
AND EXPERIMENTALLY OBSERVED VELOCITY LOSSES

| Shape | Shot No. | Mass (g) | Impact Velocity (cm/sec) | Velocity Loss Determined Experimentally (cm/sec) | Velocity Loss Predicted by Thomson Theory (cm/sec) | Velocity Loss Predicted by Nishiwaki Theory (cm/sec) |
|----------|----------|----------|--------------------------|--|--|--|
| Cone | 22 | 19.78 | 5.31×10^4 | 3.25×10^3 | 5.73×10^2 [2.77×10^3]* | 2.24×10^3 |
| Ogive | 14 | 19.32 | 4.89×10^4 | 2.41×10^3 | 5.82×10^2 | -- |
| Cylinder | 26 | 19.87 | 4.81×10^4 | 2.66×10^3 | -- | 2.02×10^3 |
| Optimal | 12 | 19.31 | 5.19×10^4 | 2.28×10^3 | 5.44×10^2 | -- |
| Russian | 25 | 19.80 | 4.98×10^4 | 2.64×10^3 | [1.5×10^3]* | -- |

*The bracketed values were calculated by Good while all other values are due to Fields. (1) The static yield strength was used in the Thomson formula to obtain the values shown in this table.

IV. NUMERICAL SOLUTIONS

The numerical solutions to the five experimental impact situations described in Table I are presented in this section. The numerical techniques are discussed and the material model employed is described in detail. The numerical results are then presented and compared to determine the effects of projectile shape.

4.1 NUMERICAL TECHNIQUES

The HELP code⁽³⁾ was employed to solve the five impact problems which make up the projectile shape effects study. HELP is a multi-material, two-dimensional, advanced Eulerian code for describing material response to dynamic loading. Since it is described in detail in Ref. 3, only a brief general outline of the code is presented here. In addition, those features of HELP which are specifically pertinent to the current study such as interface and free surface treatment, closing of voids and the inclusion of tracer particles which passively trace out the flow field history are discussed in more detail.

Figure 6 shows a section of a typical Eulerian grid used in the HELP calculations. Since the y-axis is an axis of symmetry, each cell actually represents the cross section of an annulus. The i- and j-lines form the vertical and horizontal cell boundaries respectively. The governing equations, i.e., conservation of mass, energy and momentum together with constitutive relations, are solved throughout the calculational mesh at time t . The process involves three phases and is well documented elsewhere.⁽³⁾ A new time increment, Δt , is then calculated and the same steps are repeated at time $t + \Delta t$. Thus the solution progresses

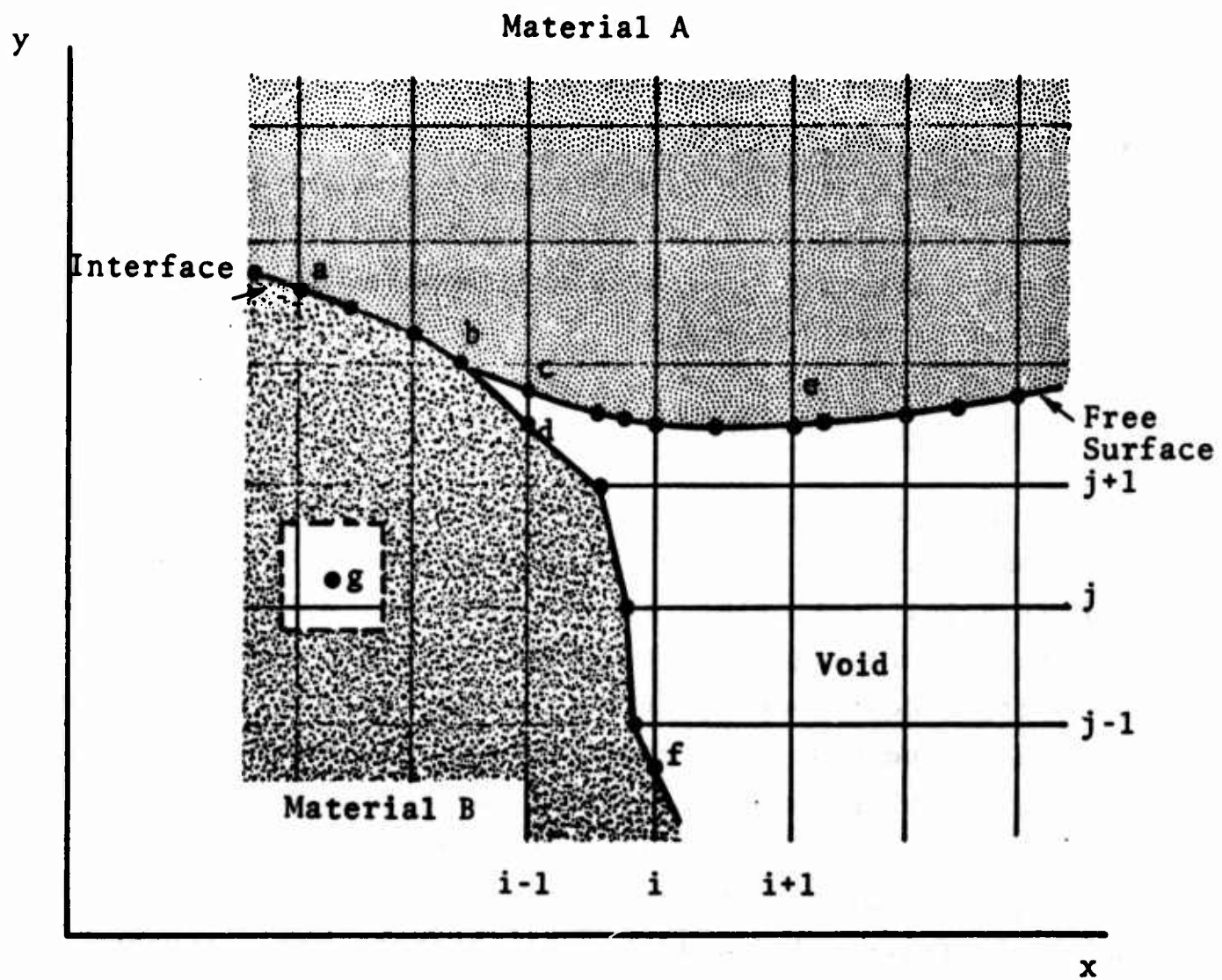


Fig. 6--Section of a typical Eulerian grid used in the HELP calculations.

incrementally in time and the material response history can therefore be established.

Special features have been incorporated into HELP to minimize certain inherent disadvantages of the general Eulerian technique while retaining the distinct Eulerian advantage of handling large scale material flow. For example, the grid can be seeded with passive tracer particles which move with a weighted velocity of the material in their vicinity. This allows a particular mass element, along with its associated dynamic variables, to be traced as it moves through the calculational mesh. The point *g* of Fig. 6 represents such a tracer particle. The dynamic variables associated with point *g* are calculated from weighted averages of those variables in the surrounding cells which are overlapped by the fictitious tracer particle cell shown dashed in Fig. 6. If desired, the tracer particles can be used as the nodes of a Lagrangian type net that deforms with the material.

Interface tracer particles such as point "a" of Fig. 6 are employed in the definition and propagation of material interfaces through the Eulerian grid. This represents a distinct advantage over the general Eulerian technique in that material diffusion at interfaces is not allowed. The special interface treatment is accomplished by calculating the mass flux across mixed cell boundaries for each material and imposing the restriction of like material flow across partial cell boundaries. The interface is then repositioned by moving the interface tracer particles according to a velocity weighting scheme which looks across the interface.

A similar scheme is used for free surface tracer particles such as points *e* and *f* of Fig. 6. For this case, however, a portion of the cell is void so that only the material side of the interface influences the free surface velocity weighting scheme. This scheme prevents

free surface diffusion and therefore eliminates another inherent disadvantage of the general Eulerian technique.

For the projectile shape effects study a special automatic void closing routine was incorporated into HELP. This was necessary because the nature of the pointed projectile penetration process causes initially free surface regions of both the target and projectiles to eventually become contact surfaces. Hence, two free surface tracer particles such as point c and d of Fig. 6 may later become a single interface tracer particle such as point b. This scheme is rather simple in that it mainly involves a change in the velocity weighting scheme.

The foregoing discussion emphasizes the advantages of HELP over the general Eulerian method. In addition, it describes very briefly and in a qualitative manner the general numerical scheme as well as the special features employed to handle free surfaces and material interfaces. For a very comprehensive documentation of the HELP code see Ref. 3.

4.2 MATERIAL MODEL

The material model to be used in the calculations consists of the equation of state, an expression for the deviatoric stress components, a yield criterion and a failure criterion.

The equation of state to be used is that due to J. H. Tillotson,⁽¹⁰⁾ modified to give a smooth transition between condensed and expanded states. For the condensed states, i.e., when $\rho/\rho_0 > 1$, or for any cold states, $I < I_s$, the equation has the form

$$p = p_c = \left[a + \frac{b}{\frac{I}{I_0 \eta^2} + 1} \right] I \rho + A \mu + B \mu^2 \quad (12)$$

For expanded hot states, i.e., when $\rho/\rho_0 < 1$ and $I > I'_s$ the equation of state has the form

$$p = p_E = aI\rho + \left[\frac{bI\rho}{\frac{I}{I_0\eta^2} + 1} + A\mu e^{-\beta(v/v_0-1)} \right] e^{-\alpha(v/v_0-1)^2} \quad (13)$$

A smooth transition between the condensed and expanded states is insured by a transition equation for the intermediate region defined by $I_s < I < I'_s$ and $\rho/\rho_0 < 1$. This blended portion of the equation of state has the form

$$p = \frac{(I-I_s)p_E + (I'_s-I)p_C}{I'_s - I_s} \quad (14)$$

In Eqs. (12) through (14) p , I and ρ are pressure, specific internal energy and mass density respectively, $\eta = \rho/\rho_0 = \mu + 1 = v_0/v$, and ρ_0 , a , b , I_0 , I_s , I'_s , A , B , α and β are constants for the particular material. The values of these constants for steel and aluminum are given in Table II.

The deviatoric stress increments, dS'_{ij} , are determined by using the elastic relation

$$dS'_{ij} = 2Gd\epsilon'_{ij} \quad (15)$$

where G is the modulus of rigidity and $d\epsilon'_{ij}$ are the increments of deviatoric strain. When such an increment of stress causes the yield criterion to be violated each stress component is proportionately reduced to bring the stress state normally back to the yield surface. A variable yield strength

$$Y = (K_0 + K_1\mu + K_2\mu^2) (1 - I/I_M) \quad (16)$$

can be defined to account for the increase in strength at high pressures and the decrease in strength at elevated temperatures.

The failure criterion to be employed is a simple one based upon relative volume. When the relative volume in a cell reaches a certain value which is greater than a specified maximum relative volume, that cell is said to fail and the stresses are zeroed out. Table III gives the shear moduli, yield stresses and relative volumes for failure which were used for aluminum and steel.

4.3 NUMERICAL RESULTS

The five experimental impact situations described in Table I form the basis for the numerical projectile shape effects study. The corresponding calculational matrix is given in Table IV. Since the projectile nose shape was of primary interest in the study, materials, target thicknesses and maximum projectile radii were not varied. The initial projectile kinetic energies are not identical, however, since it was of interest to duplicate the experimental conditions. The last column of Table IV indicates the number of μsec to which each solution was carried out in time.

Figure 7 is a composite of the initial projectile-target configurations employed in the current investigation. The left-hand side of each projectile represents an axis of symmetry. The relative dimensions are correctly scaled. It will be seen later that this method of presenting the projectile-target configurations provides a convenient means for comparing the relative penetration depths, regions of plate failure and projectile deformations as the solutions progress in time.


TABLE II
MATERIAL CONSTANTS FOR TILLOTSON EQUATION OF STATE

| Parameter Material | ρ_0 g/cm ³ | c | b | I_0 ergs/g | I_1 ergs/g | I_2 ergs/g | I_3 ergs/g | A dynes/cm ² | B dynes/cm ² | e | o |
|-----------------------|-------------------------------|-----|------|----------------------|-----------------------|-----------------------|-----------------------|----------------------------|----------------------------|---|---|
| Steel | 7.9 | 0.5 | 1.5 | 9.5×10^{10} | 2.44×10^{10} | 10.2×10^{10} | 1.26×10^{12} | 1.26×10^{12} | 1.05×10^{12} | 5 | 5 |
| Aluminum | 2.7 | 0.5 | 1.63 | 5.0×10^{10} | 3.0×10^{10} | 15.0×10^{10} | 0.75×10^{12} | 0.75×10^{12} | 0.65×10^{12} | 5 | 5 |

TABLE III
ELASTIC MODULI, YIELD STRENGTHS AND FAILURE CRITERIA

| Parameter Material | C dynes/cm ² | K_0 dynes/cm ² | K_1 dynes/cm ² | K_2 dynes/cm ² | I_M ergs/g | $(\frac{V}{V_0})_{MAX}$ |
|-----------------------|----------------------------|--------------------------------|--------------------------------|--------------------------------|----------------------|-------------------------|
| Steel | 1.93×10^{12} | 12.25×10^9 | 0 | 0 | 3.0×10^{10} | 1.03 |
| Aluminum | 2.74×10^{11} | 6.9×10^9 | 0 | 0 | 7.0×10^9 | 1.015 |

TABLE IV
BALLISTIC IMPACT CALCULATION MATRIX

| Problem Number | Projectile Nose Shape |  | Geometrical Parameters | Projectile Mass (g) | Impact Velocity (cm/sec) | Material Projectile/Target | Target Thickness (cm) | Time Duration of MILP Solution (msec) |
|----------------|-----------------------|---|---|---------------------|--------------------------|----------------------------|-----------------------|---------------------------------------|
| 100 AI | Cone | $\gamma = \frac{R}{L} \pi$ | $R = 0.355$ $L = 0.355$ | 19.78 | $5.51 \cdot 10^4$ | Steel/AI | 0.317 | 20 |
| 200 AI | Ogive | $\gamma = \sum_{i=1}^3 a_i x_i^4$ | $a_0 = 3.07 \cdot 10^{-3}$ $a_1 = 0.720$ $a_2 = -0.348$ $a_3 = 0.22 \cdot 10^{-2}$ | 19.22 | $4.09 \cdot 10^4$ | Steel/AI | 0.317 | 20 |
| 300 AI | Cylinder | $\gamma = R$ | $R = 0.355$ | 19.07 | $4.01 \cdot 10^4$ | Steel/AI | 0.317 | 20 |
| 400 AI | Cylinder | $\gamma = R \left(\frac{L}{R} \right)^{3/4}$ | $R = 0.355$ $L = 3.07$ | 19.21 | $5.19 \cdot 10^4$ | Steel/AI | 0.317 | 20 |
| 500 AI | Section | $\gamma = \sum_{i=1}^5 a_i (x-a)^4 + 0$ | $a_3 = 2.00 \cdot 10^{-4}$ $a_2 = 0.44 \cdot 10^{-3}$ $a_1 = -0.94 \cdot 10^{-2}$ $a_0 = 4.35 \cdot 10^{-1}$ $a_4 = 3.00 \cdot 10^{-1}$ $a_5 = 1.07$ $a_6 = -1.97$ $a_7 = 0.36 \cdot 10^{-1}$ $a_8 = 7.77 \cdot 10^{-2}$ $a_9 = -3.10 \cdot 10^{-4}$ | 19.00 | $4.96 \cdot 10^4$ | Steel/AI | 0.317 | 20 |

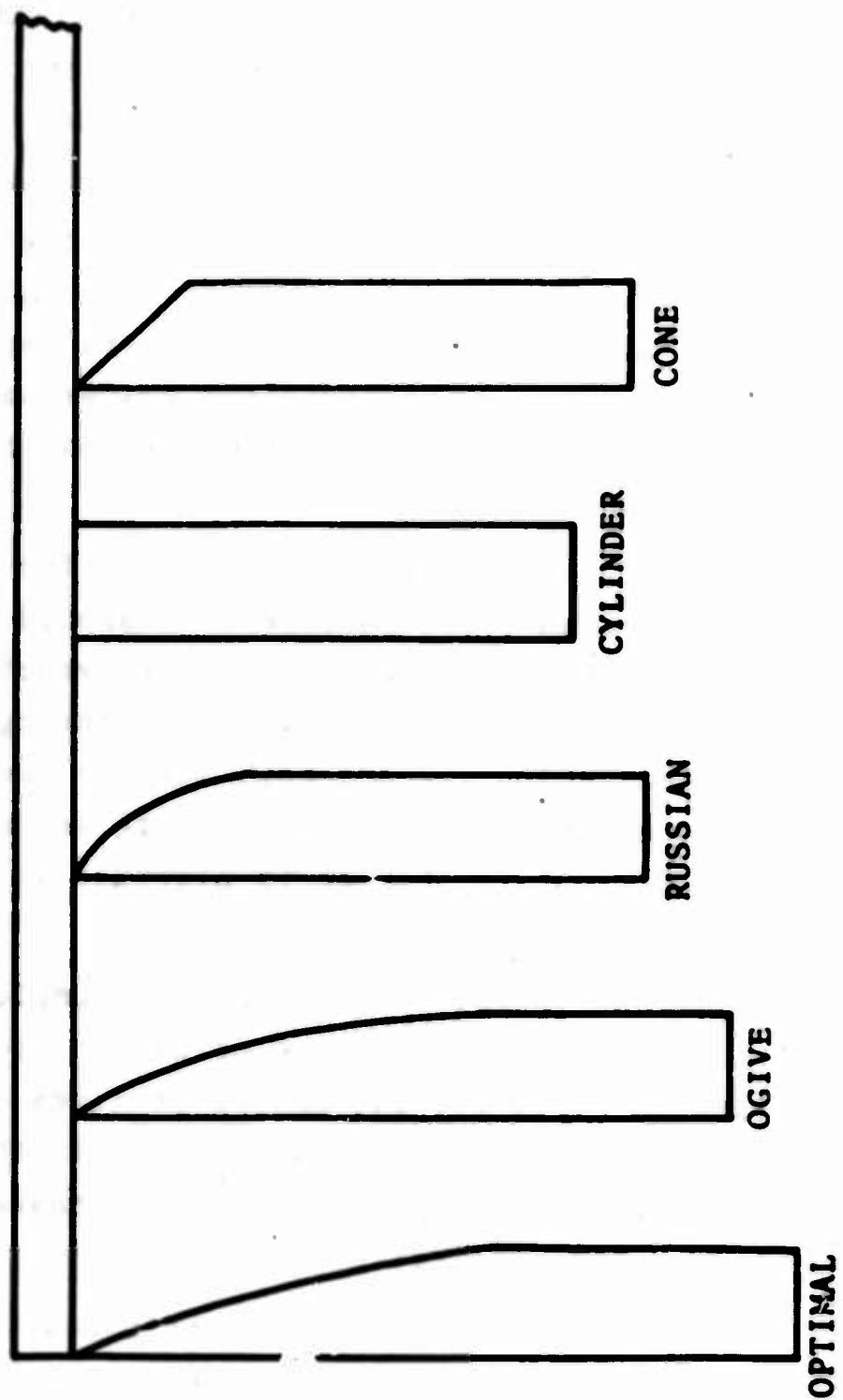


Fig. 7--Composite of initial projectile target configurations.

Since many of the general qualitative features of the five numerical solutions are similar, only the solution to the Russian projectile impact is presented in detail. The results of the other four impact problems are presented in the form of comparisons of specific quantitative data.

Figure 8 shows an SC-4020 plot of the initial configuration of the Russian projectile impact problem and the Eulerian grid employed in the solution. For clarity in subsequent plots the grid is not included. These plots represent a connection of the free surface and interface tracer particles and hence supply the projectile-target configurational history throughout the perforation process.

Figure 9 shows the configuration at 2 μ sec. The shaded area indicates a region of material failure. It should be noted that plate failure begins along the axis of symmetry at the rear free surface of the plate. Figures 9 through 12 indicate that the failed region spreads both axially and radially indicating petalling failure. A complete set of the configurational plots out to 36 μ sec is provided in the Appendix.

Because it would be impractical to include complete sets of configurational plots for all five solutions, comparisons are provided in Figs. 13, 14, and 15 at times of 10, 15 and 20 μ sec respectively. The dashed lines in these figures indicate the initial configuration and the shaded areas denote regions of material failure.

In Fig. 16 the final calculated projectile configurations are compared with their undeformed shapes. The times corresponding to each of these configurations are given in Table IV.

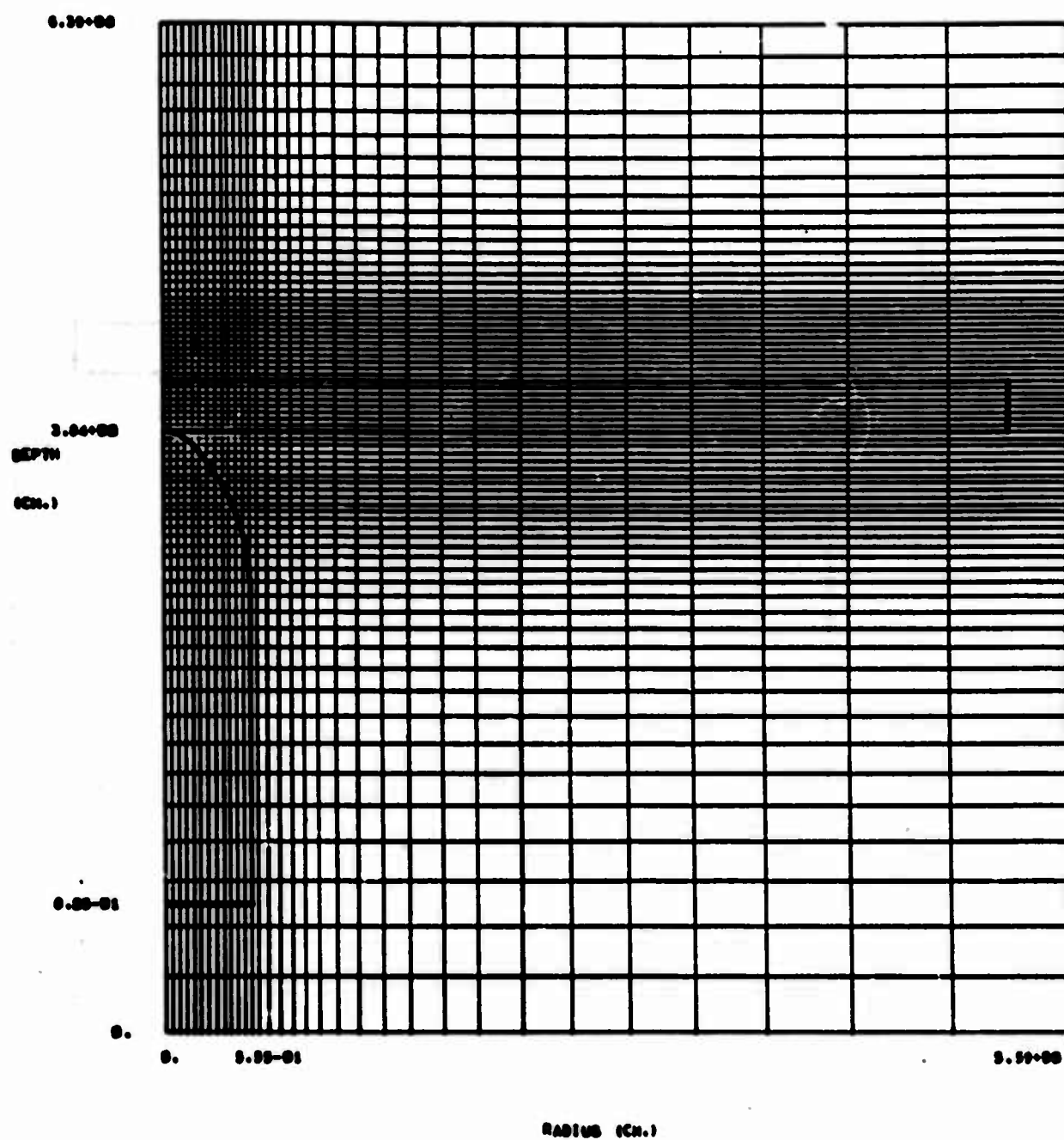


Fig. 8--Initial configuration and computational grid for the Russian projectile impact calculation.

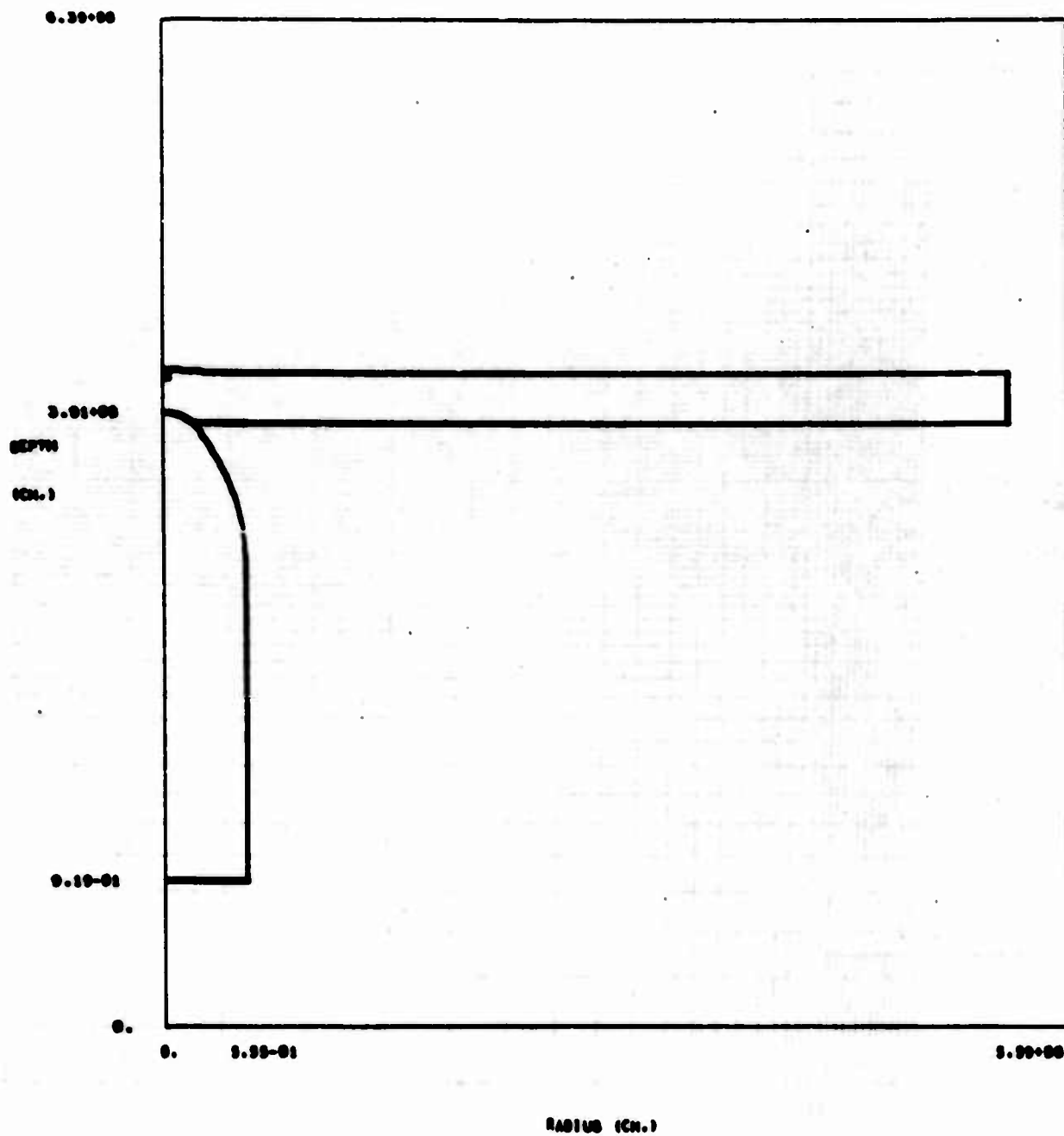


Fig. 9--Russian projectile-target configuration at 2 μ sec.

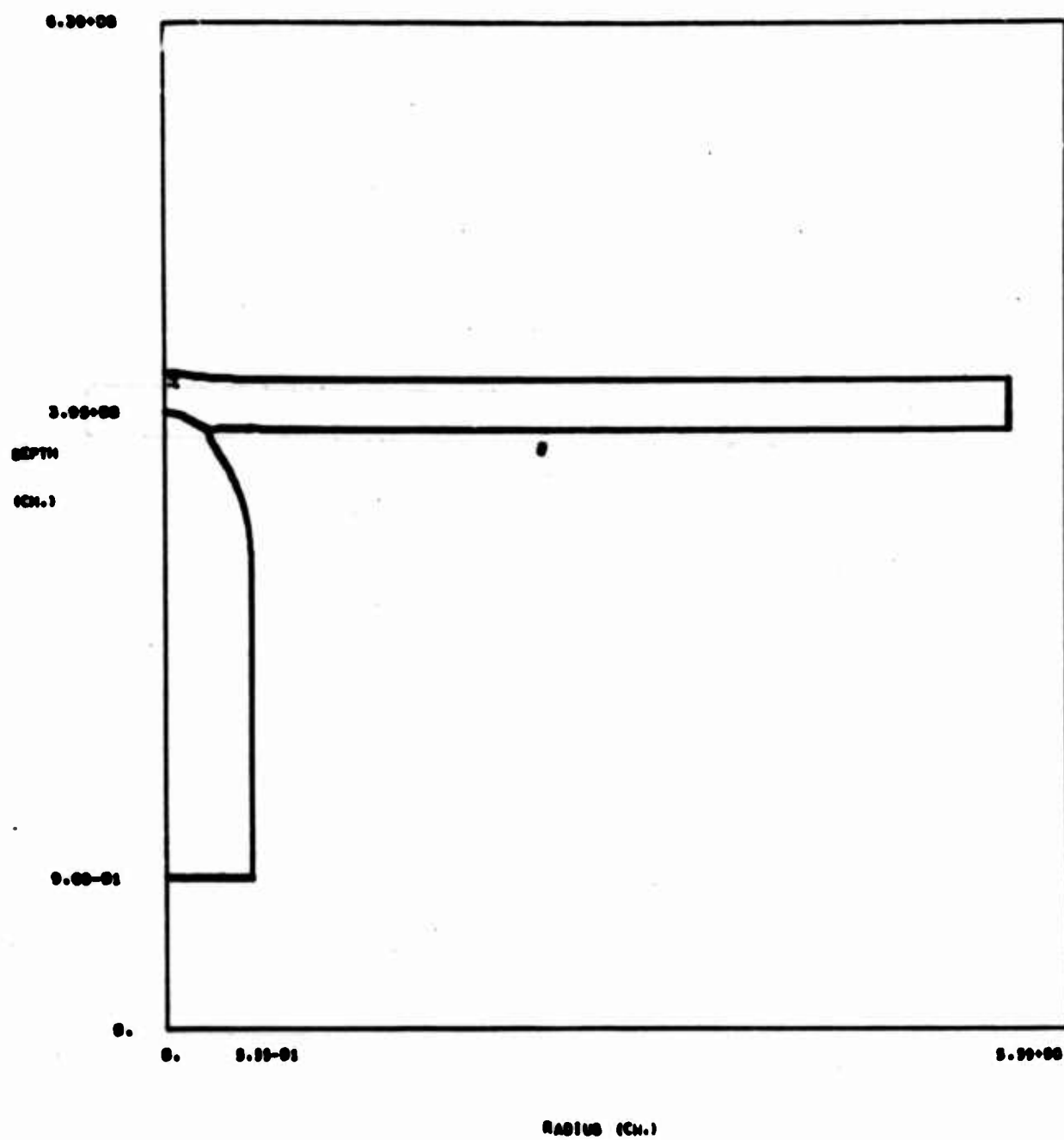


Fig. 10--Russian projectile-target configuration at 3 μ sec.

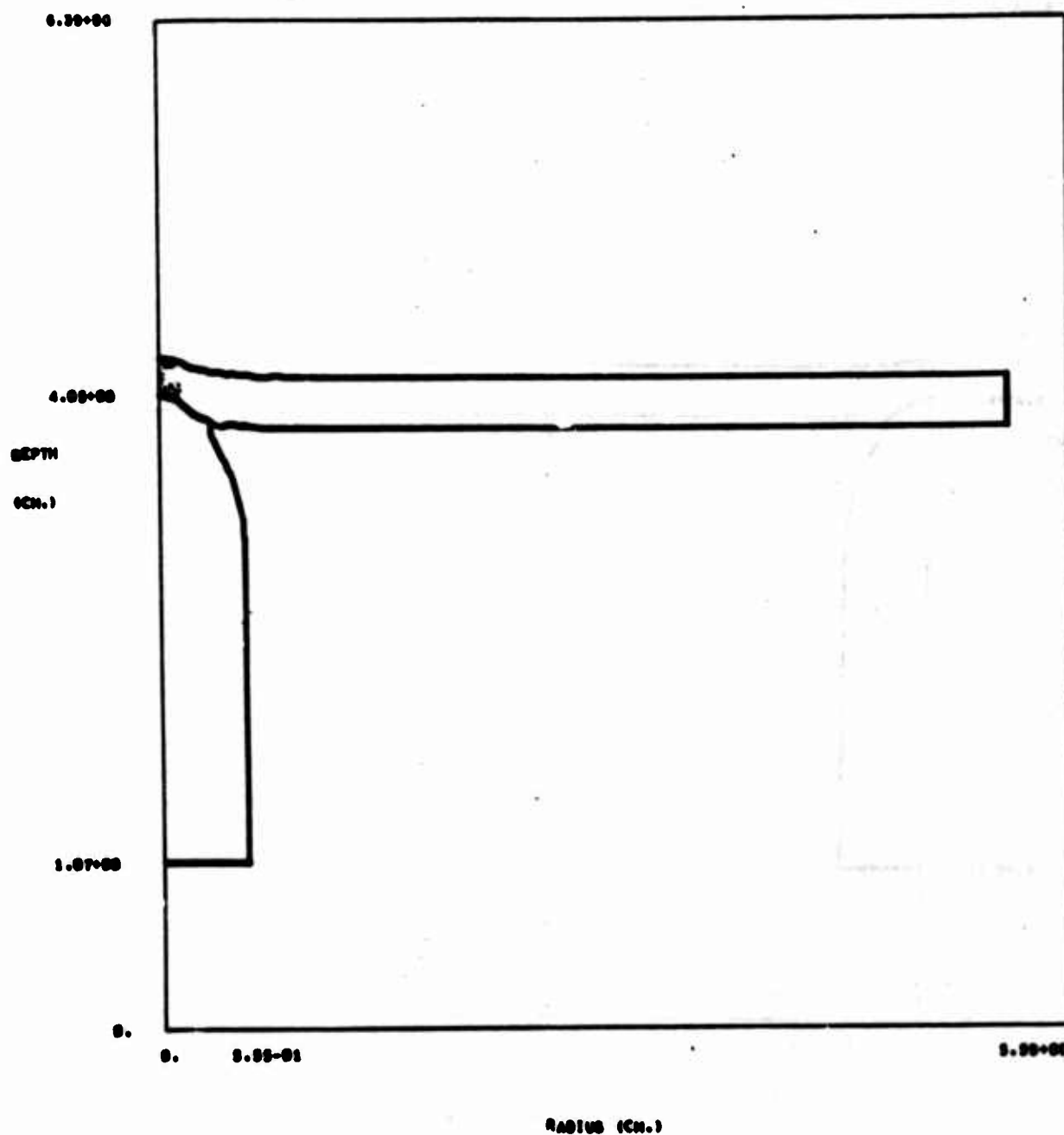


Fig. 11--Russian projectile-target configuration at 5 μ sec.

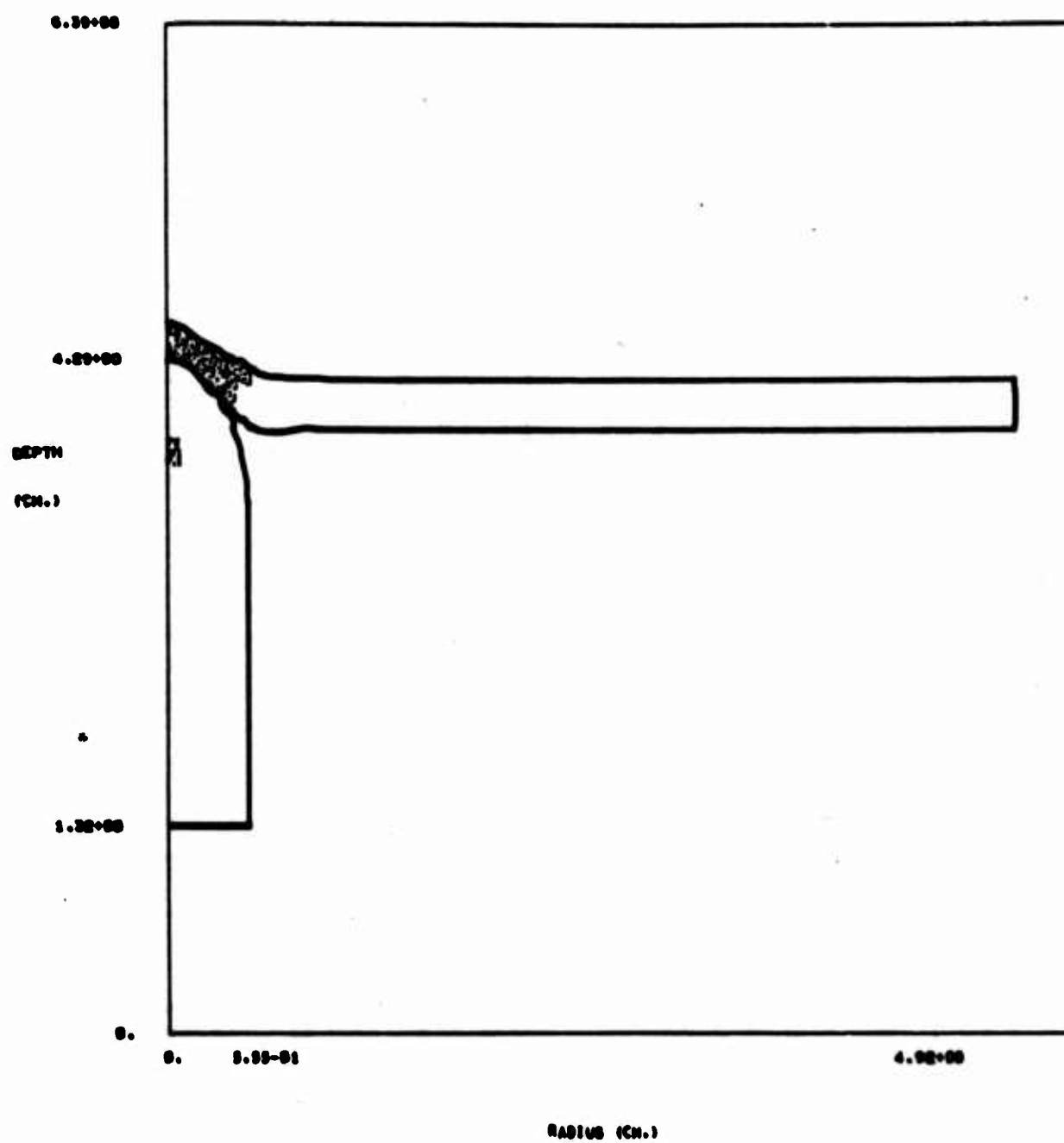


Fig. 12--Russian projectile-target configuration at 10 μ sec.

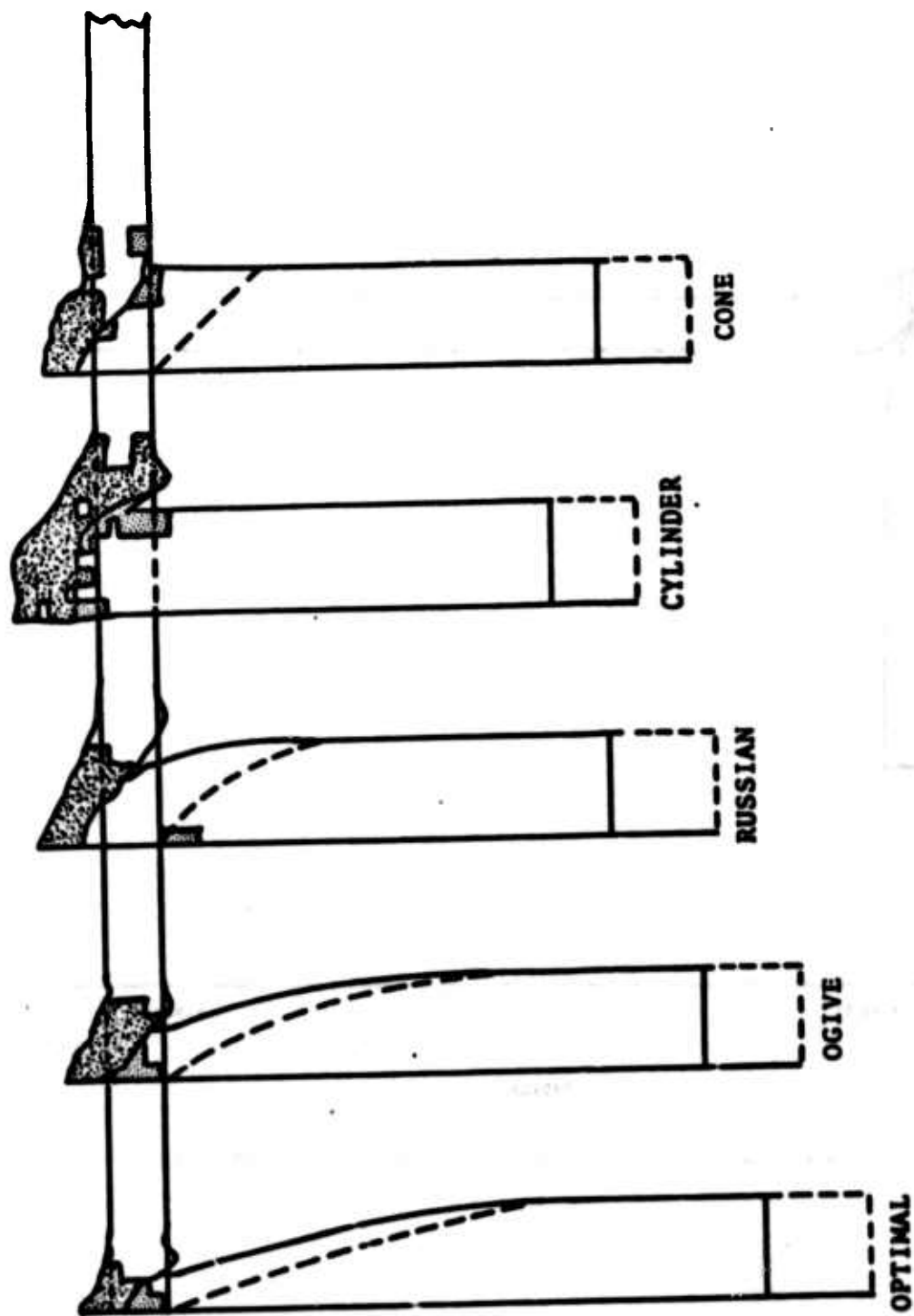


Fig. 13--Comparison of projectile-target configurations at $t = 10 \mu\text{sec}$.

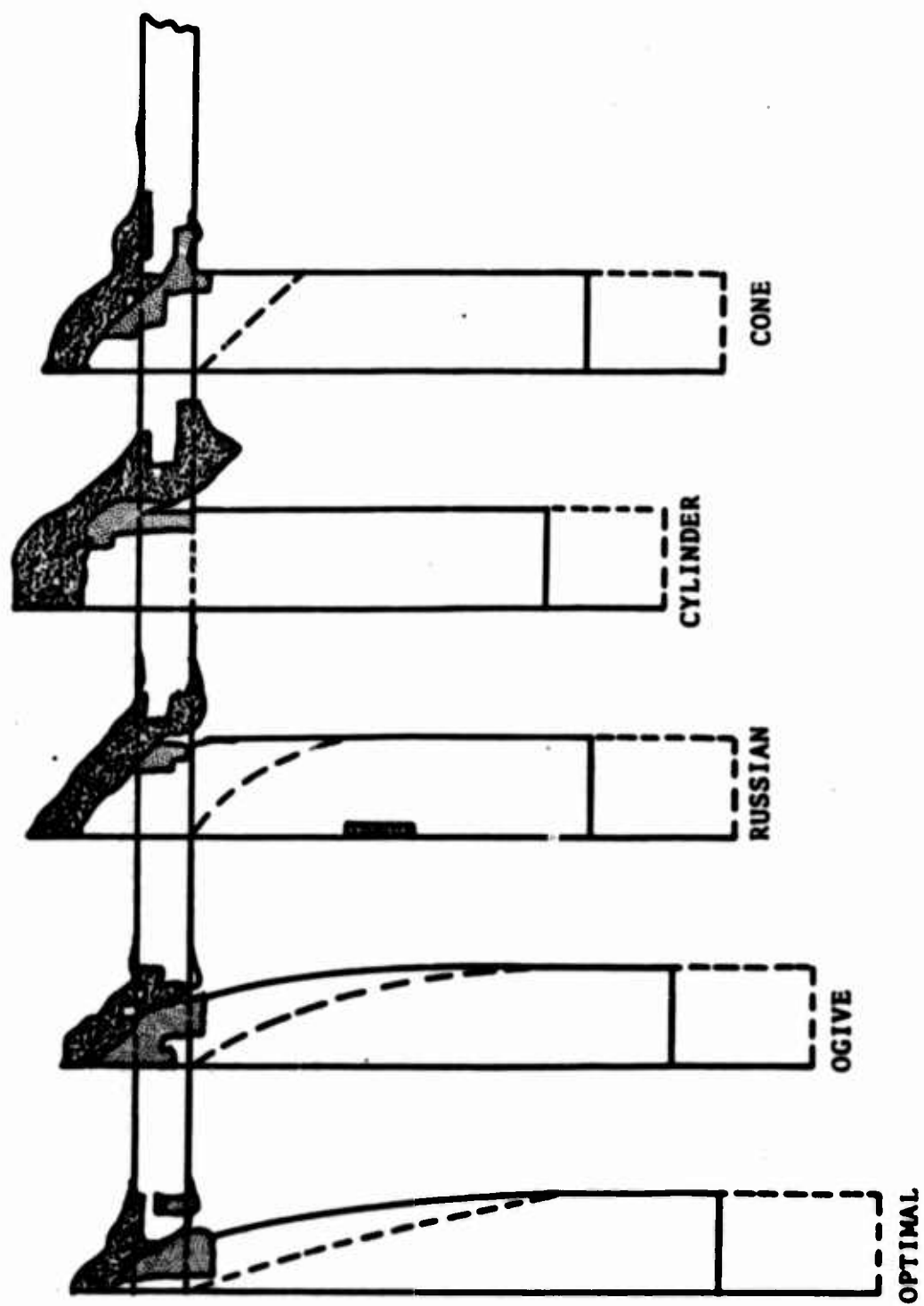


Fig. 14--Comparison of projectile-target configurations at $t = 15 \mu\text{sec}$.

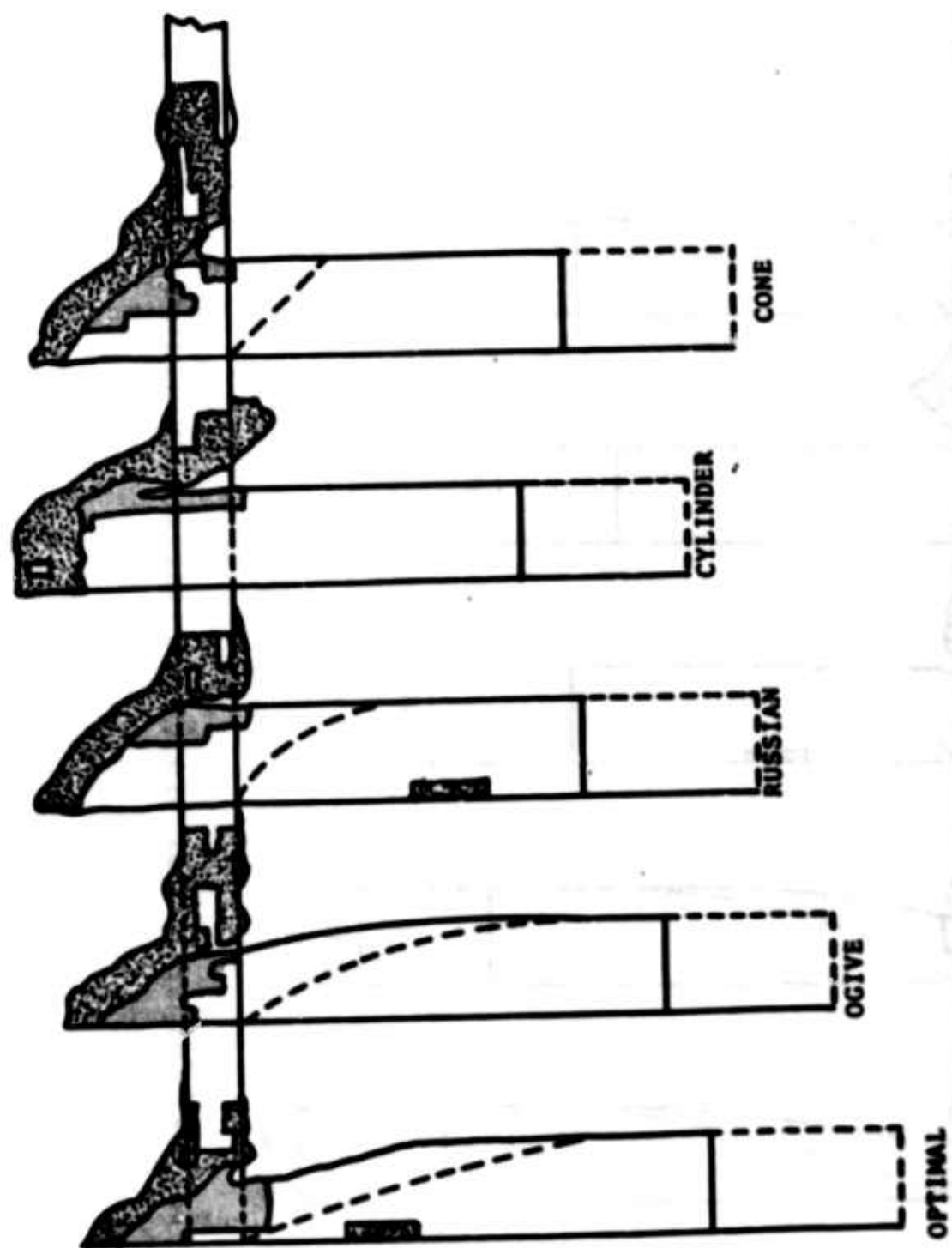


Fig. 15--Comparison of projectile-target configurations at $t = 20 \mu\text{sec}$.

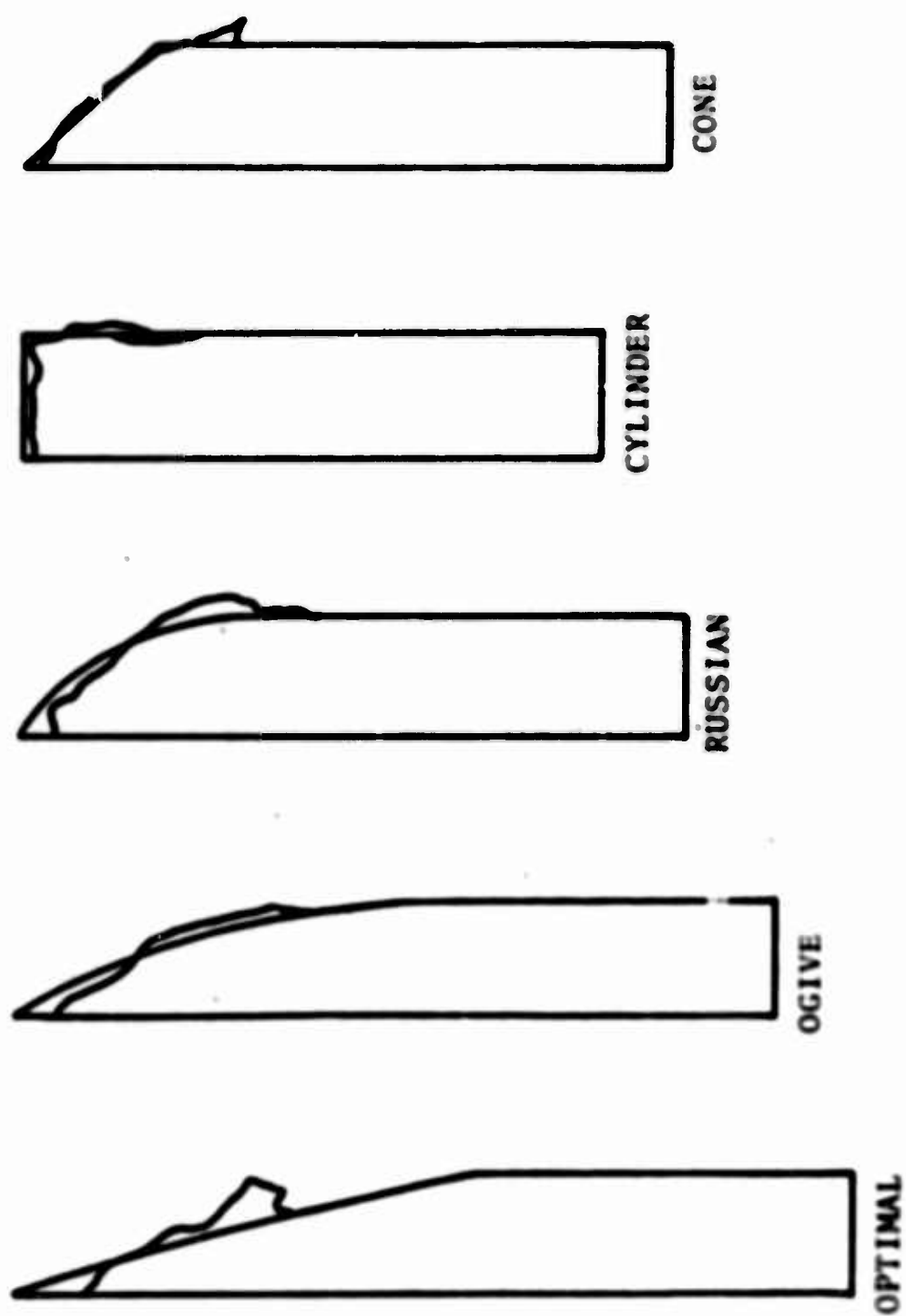


Fig. 16--Comparison of final calculated projectile configurations.

V. DISCUSSION OF RESULTS

It is of interest to compare the numerical results with both perforation formula predictions and experimental observations. Figure 17 is a plot of normalized projectile kinetic energy versus time. The experimentally observed residual kinetic energy of the projectile, E_R , has been subtracted from the numerically predicted projectile kinetic energy, $(KE)_p$. This difference has been divided by the experimentally observed loss in projectile kinetic energy, $E_0 - E_R$, to obtain the ordinate for the plot of Fig. 17. Plotted versus time, this quantity should, for all projectile shapes, have a value of unity at $t = 0$ and approach zero asymptotically at some later time, provided the HELP predictions are in agreement with experimental observations. This indeed seems to be the case, as is seen in Fig. 17. The cylindrical and conical nose projectiles attained the asymptotic values rather abruptly, due to their bluntness. The more pointed the projectile, the longer it takes to attain its correct value. This is because the projectile must travel a greater distance before the maximum projectile radius is in contact with the plate. The Russian projectile calculation was carried out to 36 μ sec before it approached its asymptotic value. It became apparent that the calculations involving the extremely pointed ogive and optimal projectiles, would therefore have to be carried out in time considerably further than 36 μ sec. Because of the additional computing time necessary to carry out such long calculations, it was decided to stop the ogive and optimal projectile calculations at 29 μ sec. Based on the fact that the numerically calculated cylindrical-, conical-, and Russian-shaped projectile kinetic energies all attained their respective experimentally observed values, it is believed that this would also be the case if the ogive and optimal impact calculations were continued.

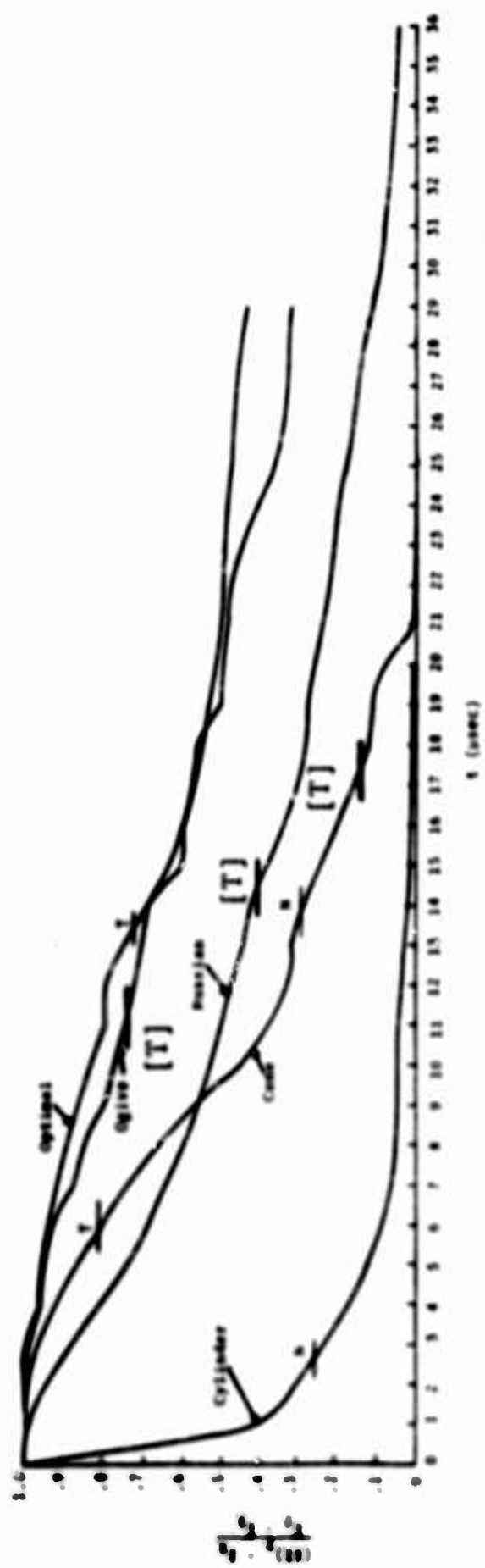


Fig. 17--Normalized projectile kinetic energy versus time. The T's and N's indicate Thomson and Nishiwaki theory predictions. The bracketed values were calculated by Good. The static yield strength was used in the Thomson theory.

The horizontal lines on Fig. 17 labeled T and N indicate the Thomson and Nishiwaki theory predictions. If the perforation formula predictions were in complete agreement with the experimental observations, the lines would all lie on the time axis, i.e., they would have zero ordinate values. Thus, Fig. 17 indicates that the numerical predictions of residual kinetic energy are in excellent agreement with experiment but that the Thomson and Nishiwaki theories show considerable discrepancy. The values of T and N shown in Fig. 17 were calculated by Fields⁽¹⁾ using the static yield strength of the plate material. The bracketed values were calculated by Good using the Thomson theory and for the case of the conical projectile there is considerable disagreement with Fields' value.

In Fig. 18 the percent loss in projectile kinetic energy is plotted for the various projectile shapes, beginning with the most efficient penetrator. The solid circles represent the experimentally observed values. The open circles represent the HELP predictions. As expected from the data presented in Fig. 17, the percent loss in projectile kinetic energy, as predicted by the HELP calculations, for the cylindrical and relatively blunt conical head projectiles are in good agreement with experiment while the more pointed projectiles are not. This, of course, is due to the fact that the more pointed projectile impact solutions were not carried out sufficiently far in time. It should be mentioned that conversion of projectile kinetic energy into internal energy was still taking place in the pointed projectiles when the calculations were stopped. Since the loss in projectile kinetic energy can go into projectile internal energy as well as target kinetic or internal energy, energy partitioning is of interest. Figure 18 shows the numerically predicted energy partitioning by means of shaded regions.

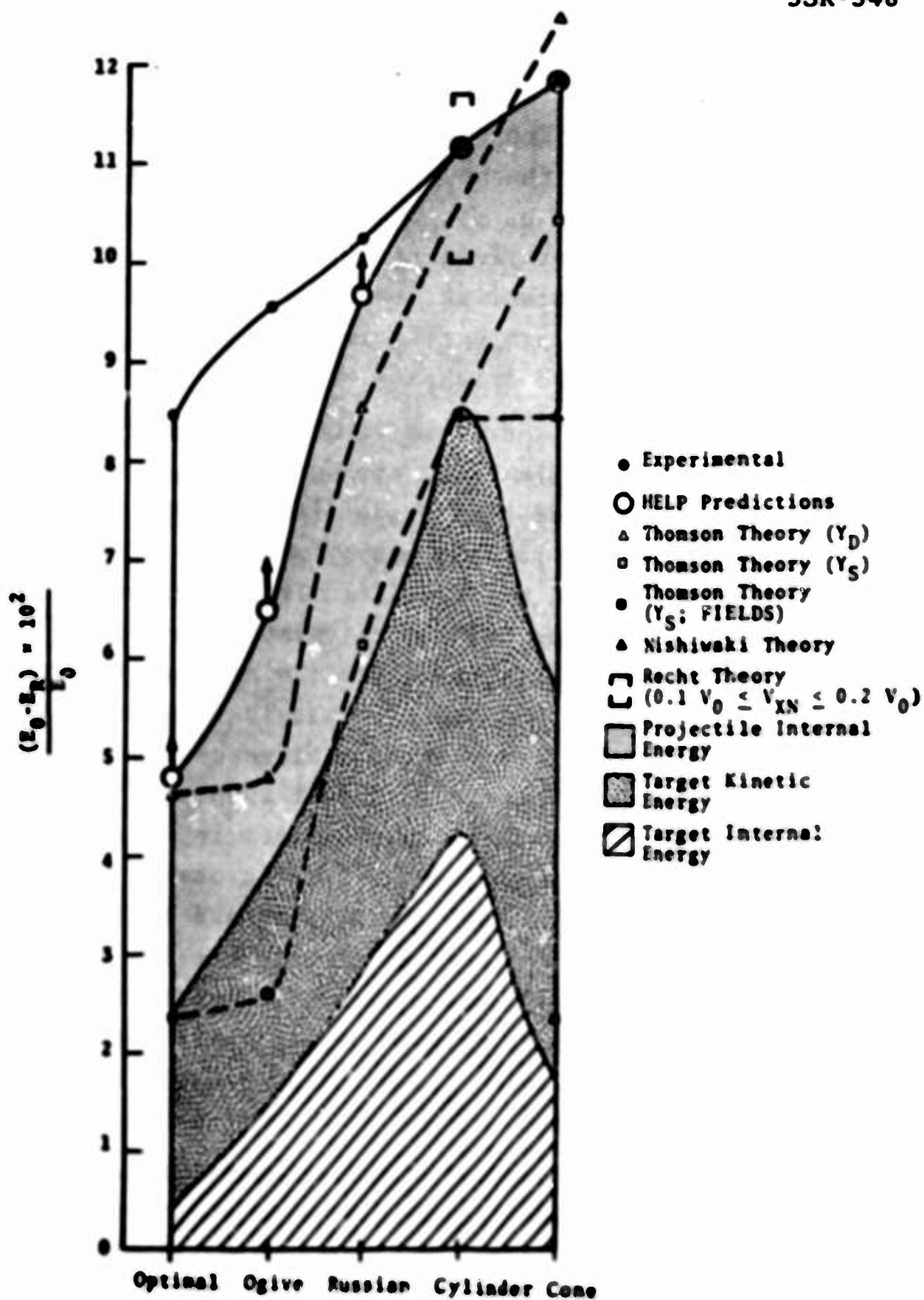


Fig. 18--Percent loss in projectile kinetic energy for the various projectile shapes. The arrows attached to the open circles indicate that the calculated projectile kinetic energies were still decreasing when the calculations were terminated.

The broken lines connecting the open triangles and squares in Fig. 18 show the percent reduction of projectile kinetic energy predicted by the Thomson theory using the dynamic and static target yield strengths respectively. The predictions of the Nishiwaki theory are shown for the cylindrical and conical projectile impacts by the dashed line connecting the solid triangles.

The solid square shows the value predicted by the Thomson theory with static yield strength as reported by Fields⁽¹⁾ for the conical head projectile impact. The value of percent reduction in kinetic energy obtained by Good who applied the same formula was considerably greater as evidenced in Fig. 18. Since Fields did not calculate energy loss for the Russian projectile, his value for the conical projectile lead him to state that "Preliminary calculations using the Thomson theory predicted very small differences in perforation velocity loss between the different shapes." ⁽¹⁾ The dashed line which connects the open squares in Fig. 18 shows that the percent loss in projectile kinetic energy predicted by the Thomson theory for both the Russian and conical projectile shapes indicate disagreement with Fields' statement. It is concluded that the Thomson theory is sensitive to projectile shape for the four pointed impact cases reported here, but that the predicted values of projectile energy loss are low.

The residual velocity for the cylindrical impact case calculated by Heyda's formula is 4.43×10^4 cm/sec as compared to 4.61×10^4 cm/sec predicted by Nishiwaki's formula and 4.5×10^4 cm/sec predicted by Recht's formula using a ballistic limit of 1.02×10^4 cm/sec. The experimentally observed value of residual velocity of the cylinder was 4.54×10^4 cm/sec. Although Recht's formula seems to be closest to the observed value for this case, the total spread

in predicted velocities is less than 4 percent of the observed value.

Figure 18 also provides a measure of relative penetration efficiency for the various projectile shapes. Of the five shapes investigated, the optimal-head projectile is the most efficient, followed by the ogival-, Russian-, cylindrical- and conical-head projectiles.

VI. CONCLUSIONS

Within the scope of the current investigation, available pointed projectile perforation formulas do not adequately predict residual projectile kinetic energy. HELP calculations, carried out sufficiently far in time, seem to predict values of projectile kinetic energy which asymptotically approach the observed residual energies. This agreement with experimental observations is quite encouraging, since, in addition to adding physical insight into penetration phenomena, the results demonstrate that numerical solutions can provide useful information to both weapons and armor designers, as well as to vulnerability analysts. Furthermore, the HELP code should be a useful tool in parametric studies designed especially for developing new, or altering presently available, simple perforation formulas.

REFERENCES

1. Fields, T. E., "The Effect of Projectile Shape on the Ballistic Perforation of Thin Metal Plates," AFML-TR-69-202, July 1969.
2. Hageman, L. J., and J. M. Walsh, "HELP Code Solutions to Two Test Problems in Armor Penetration," Systems, Science and Software Report 3SR-201, January 1970.
3. Walsh, J. M., et al., "HELP, a Multiple-Material Eulerian Program for Compressible Fluid and Elastic-Plastic Flows in Two Space Dimensions and Time," Systems, Science and Software Report 3SR-350, June 1970.
4. Sedgwick, R. T., "Theoretical Investigation of Metallic Perforation by Kinetic Energy Projectiles," AFATL-TR-69-54, April 1969.
5. Thomson, William T., "An Approximate Theory of Armor Penetration," J. Appl. Phys. 26:1, 80-32, January 1955.
6. Zaid, Melvin and Burton Paul, "Mechanics of High Speed Projectile Penetration," J. of Franklin Inst., 264:117-126, 1957.
7. Nishiwaki, Jien, "Resistance to the Penetration of a Bullet through an Aluminum Plate," J. Phys. Soc. of Japan, 6:374-378, October 1951.
8. Recht, R. F., and T. W. Ipson, "Ballistic Perforation Dynamics," J. Appl. Mech., 384-389, September 1963.
9. Heyda, J. F., "Ballistic Impact into Thin Plates," General Electric Co. Space Sciences Laboratory, Materials and Mechanics TM 70-002, February 1970.
10. Tillotson, J. H., "Metallic Equations of State for Hypervelocity Impact," General Atomic Report GA-3216, July 1962.

APPENDIX
RUSSIAN PROJECTILE-TARGET CONFIGURATIONS
AT VARIOUS TIMES

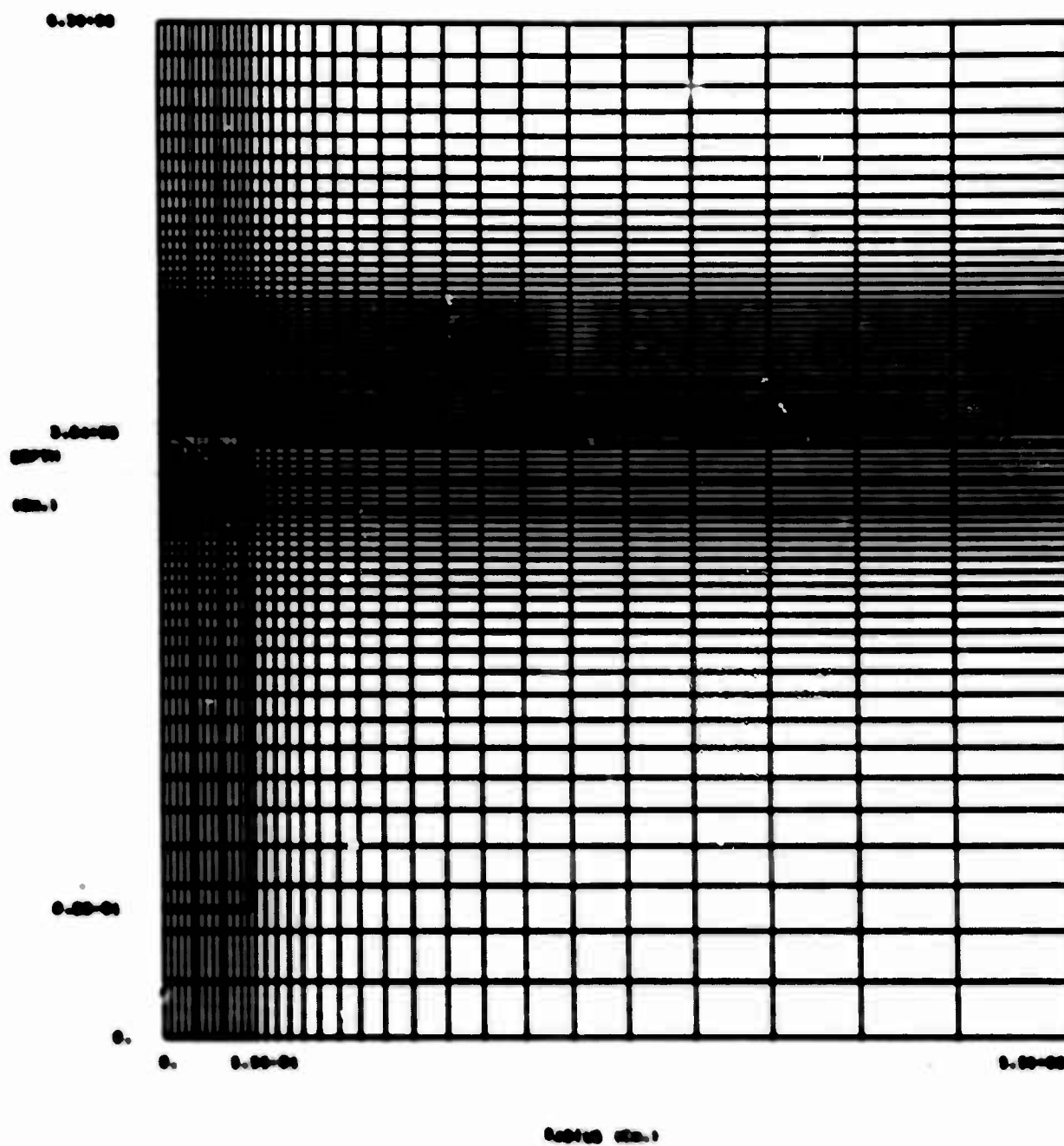


Fig. A.1--Russian projectile-target configuration at $t = 0$.

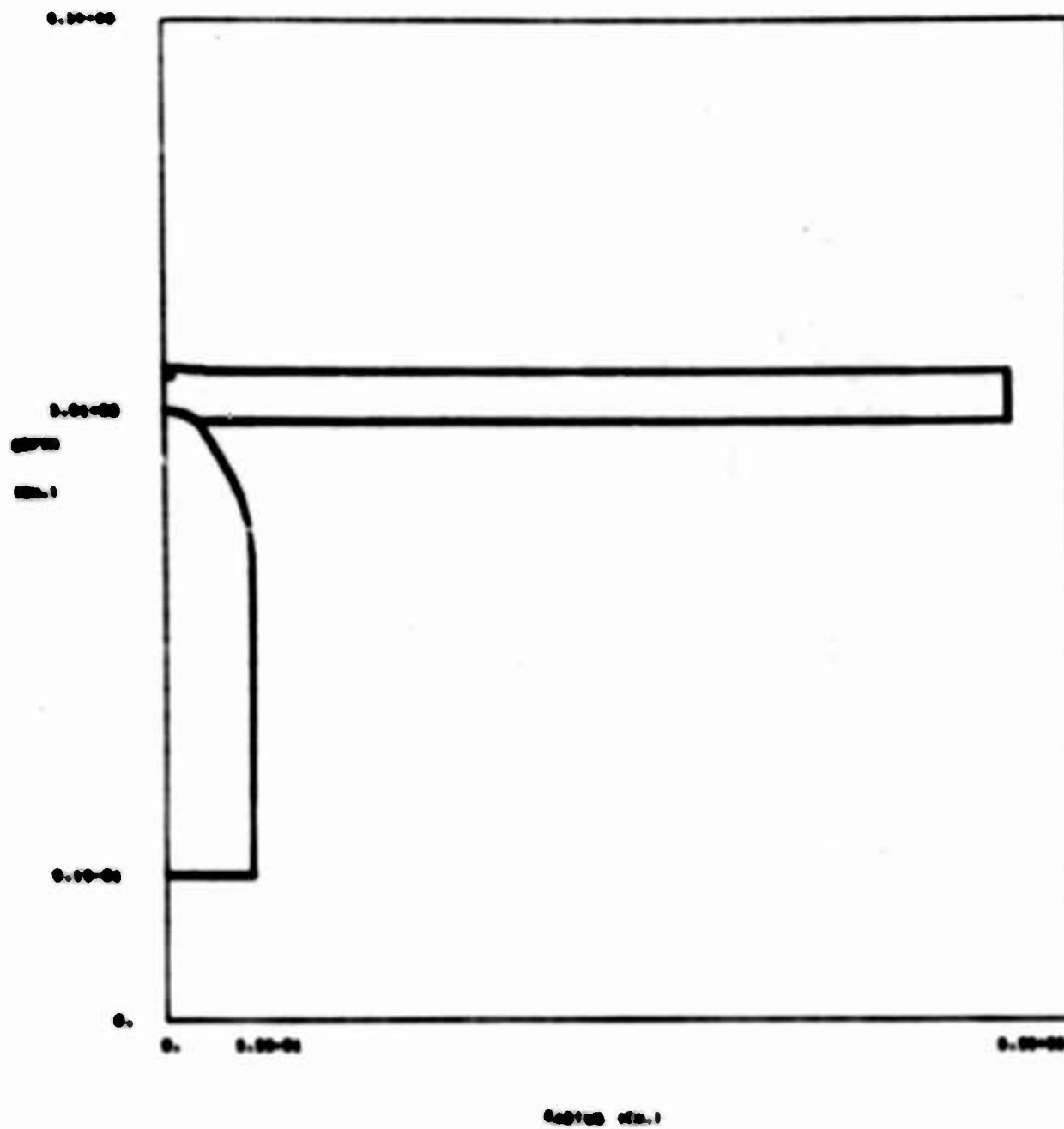


Fig. A.2--Russian projectile-target configuration
at $t = 2 \mu\text{sec.}$

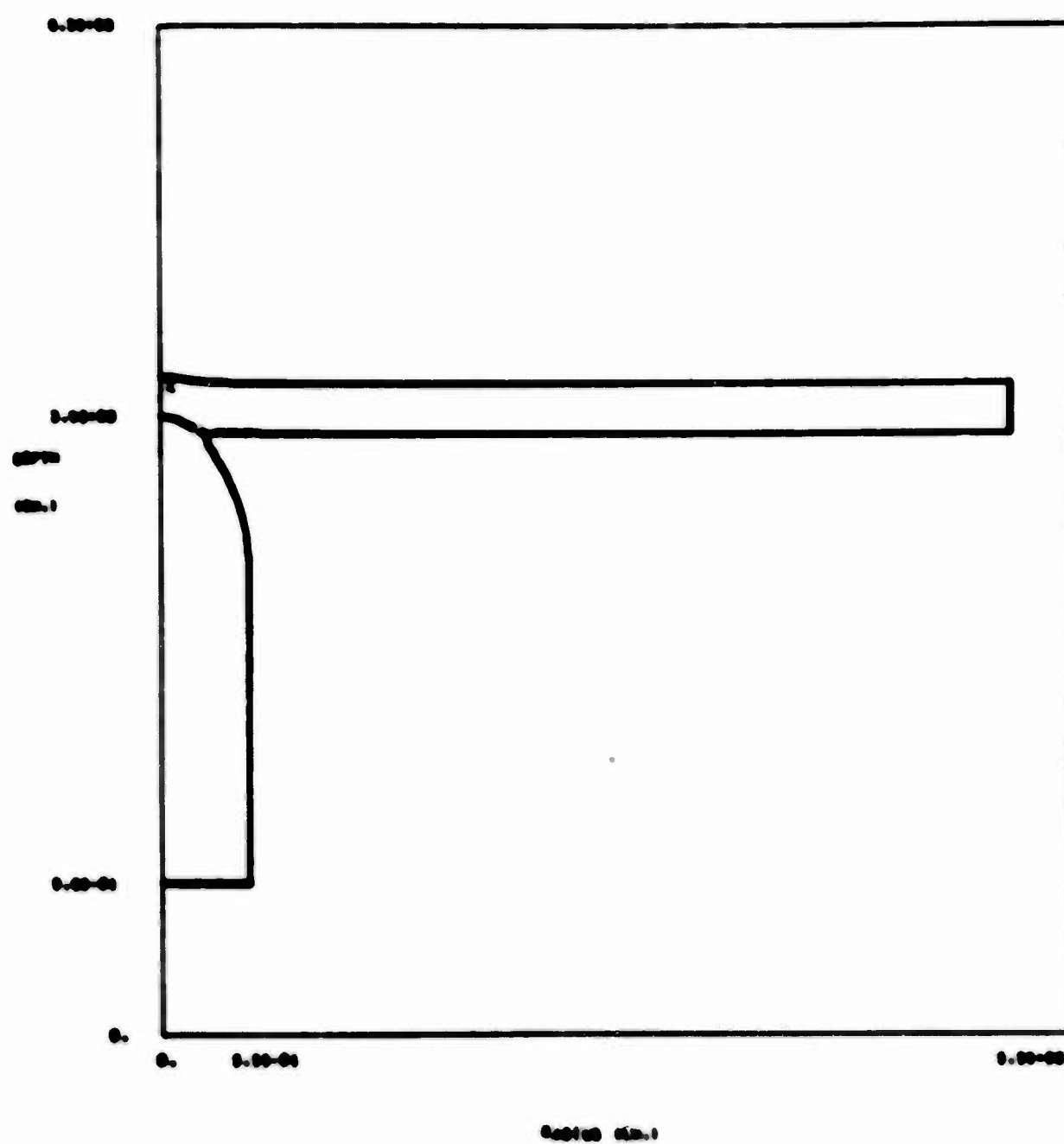


Fig. A.3--Russian projectile-target configuration
at $t = 3 \mu sec$.

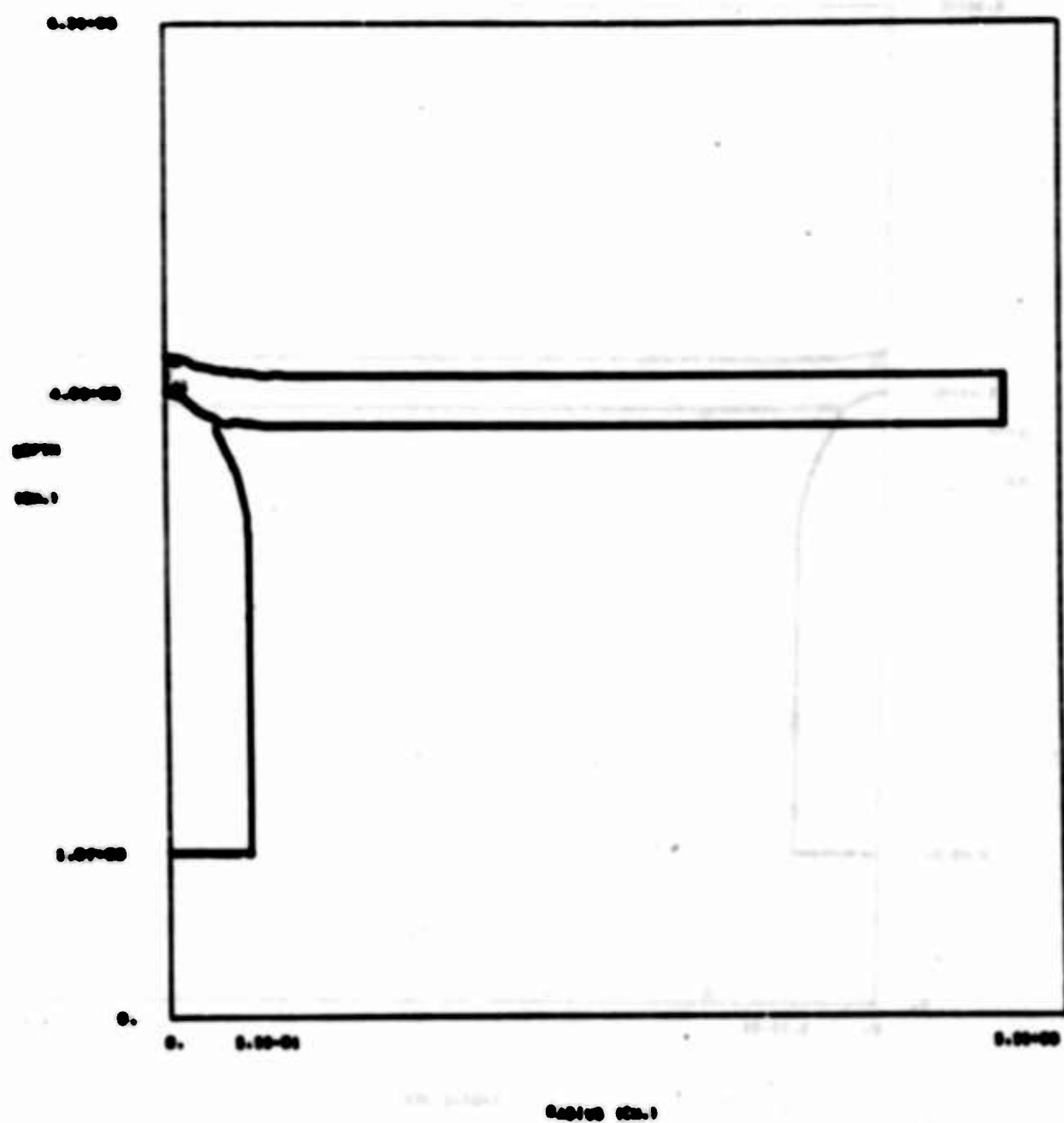


Fig. A.4--Russian projectile-target configuration
at $t = 5 \mu\text{sec}$.

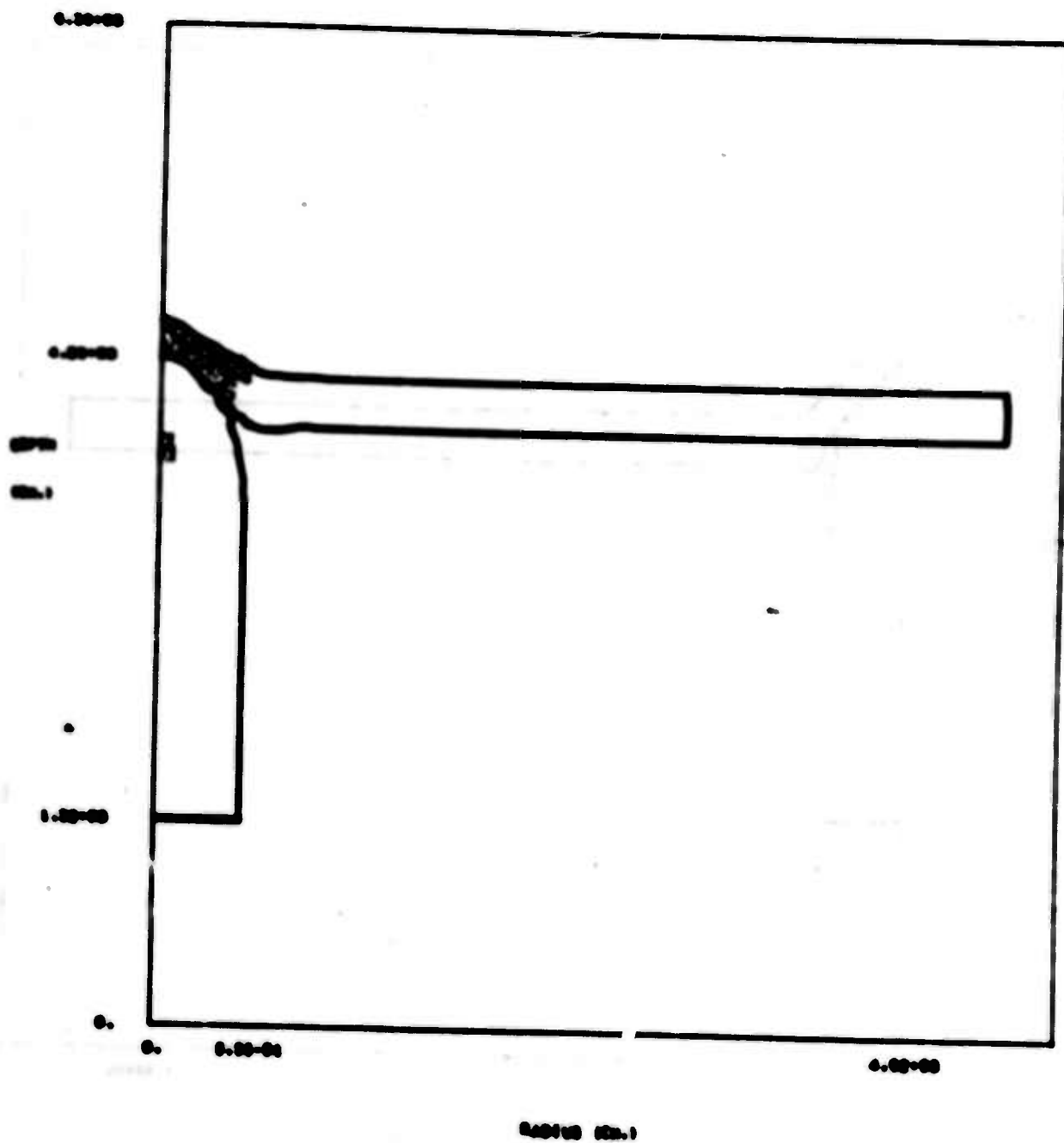


Fig. A.5--Russian projectile-target configuration
at $t = 10 \mu\text{sec.}$

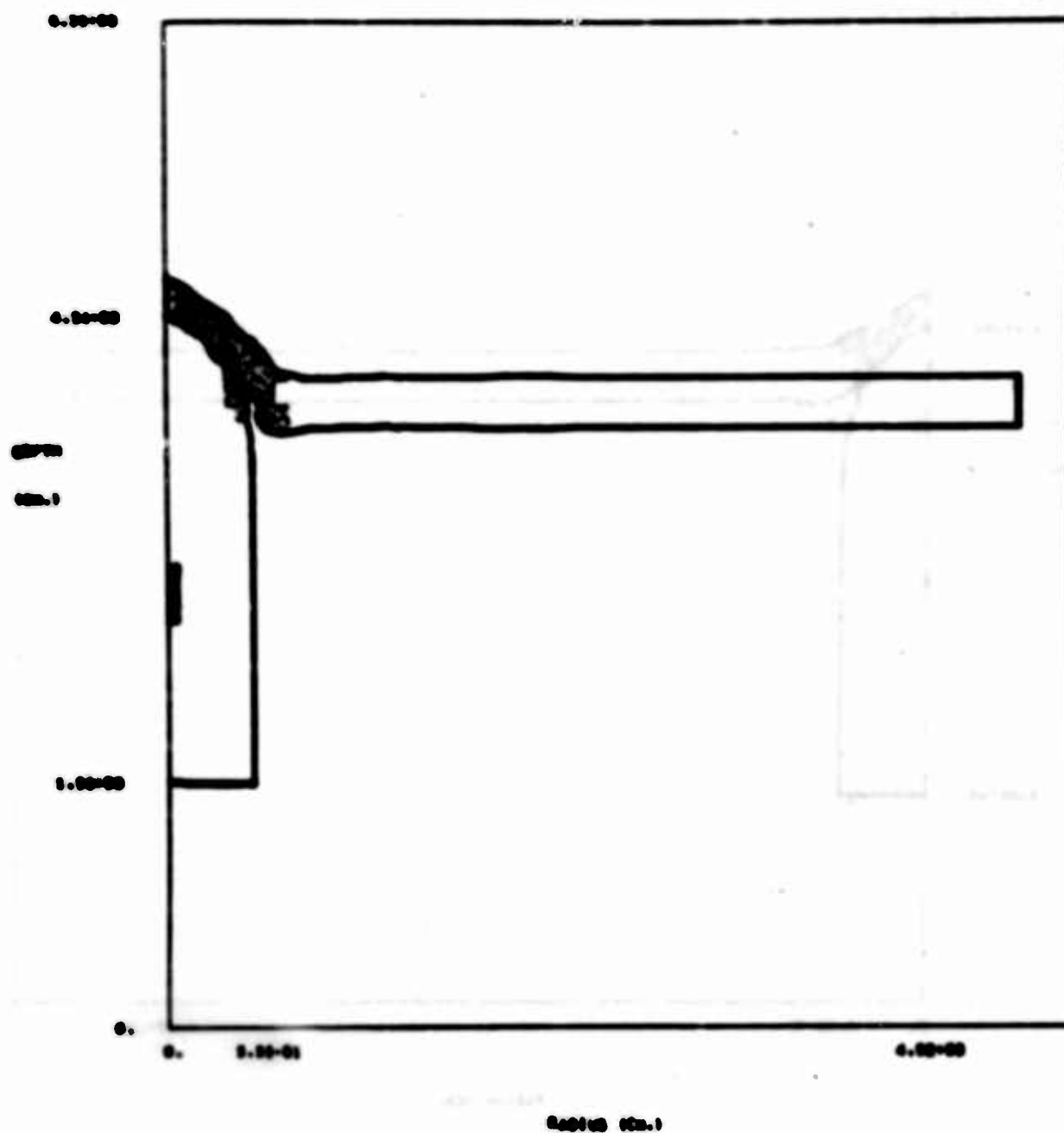


Fig. A.6--Russian projectile-target configuration
at $t = 15 \mu\text{sec.}$

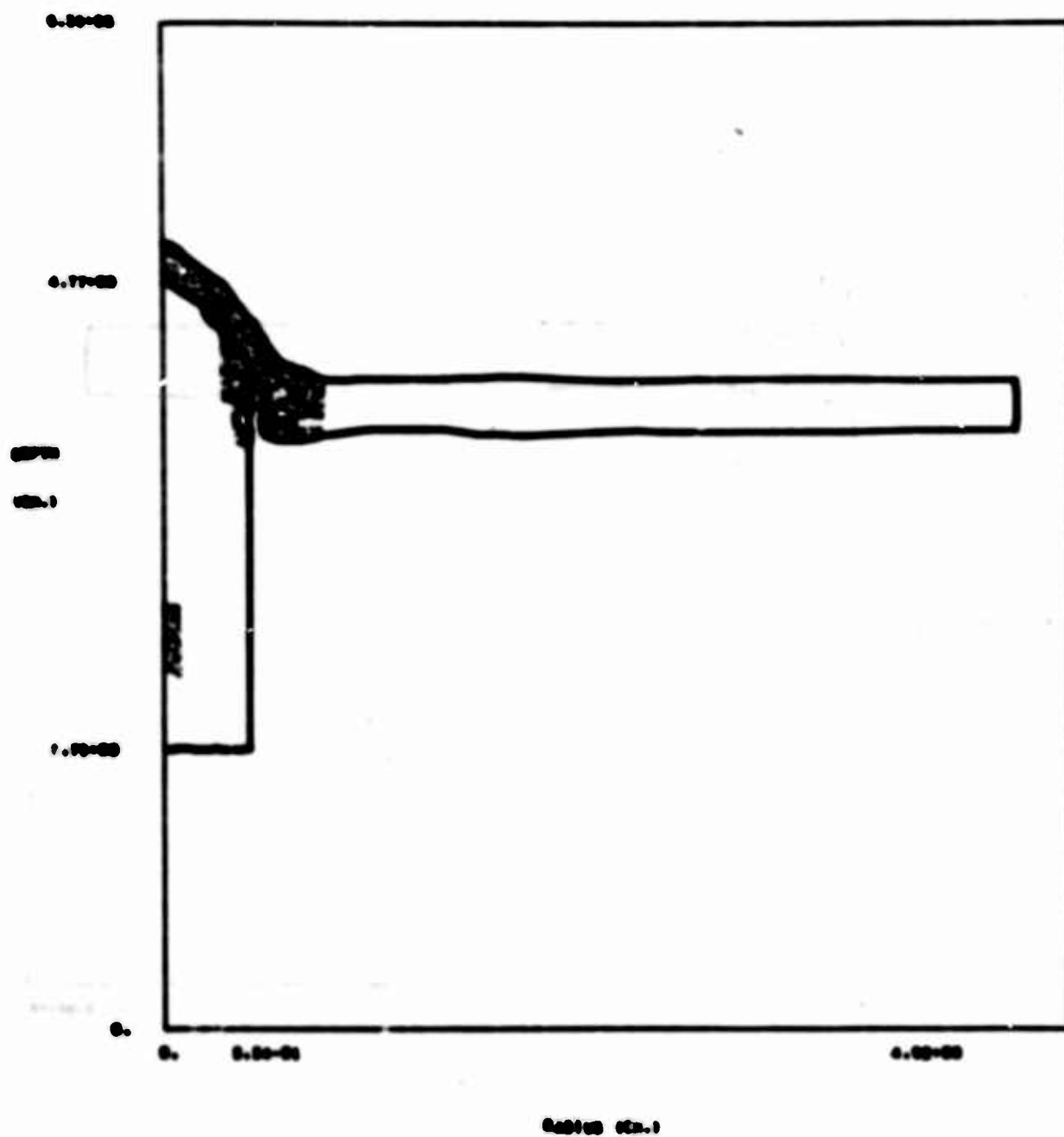
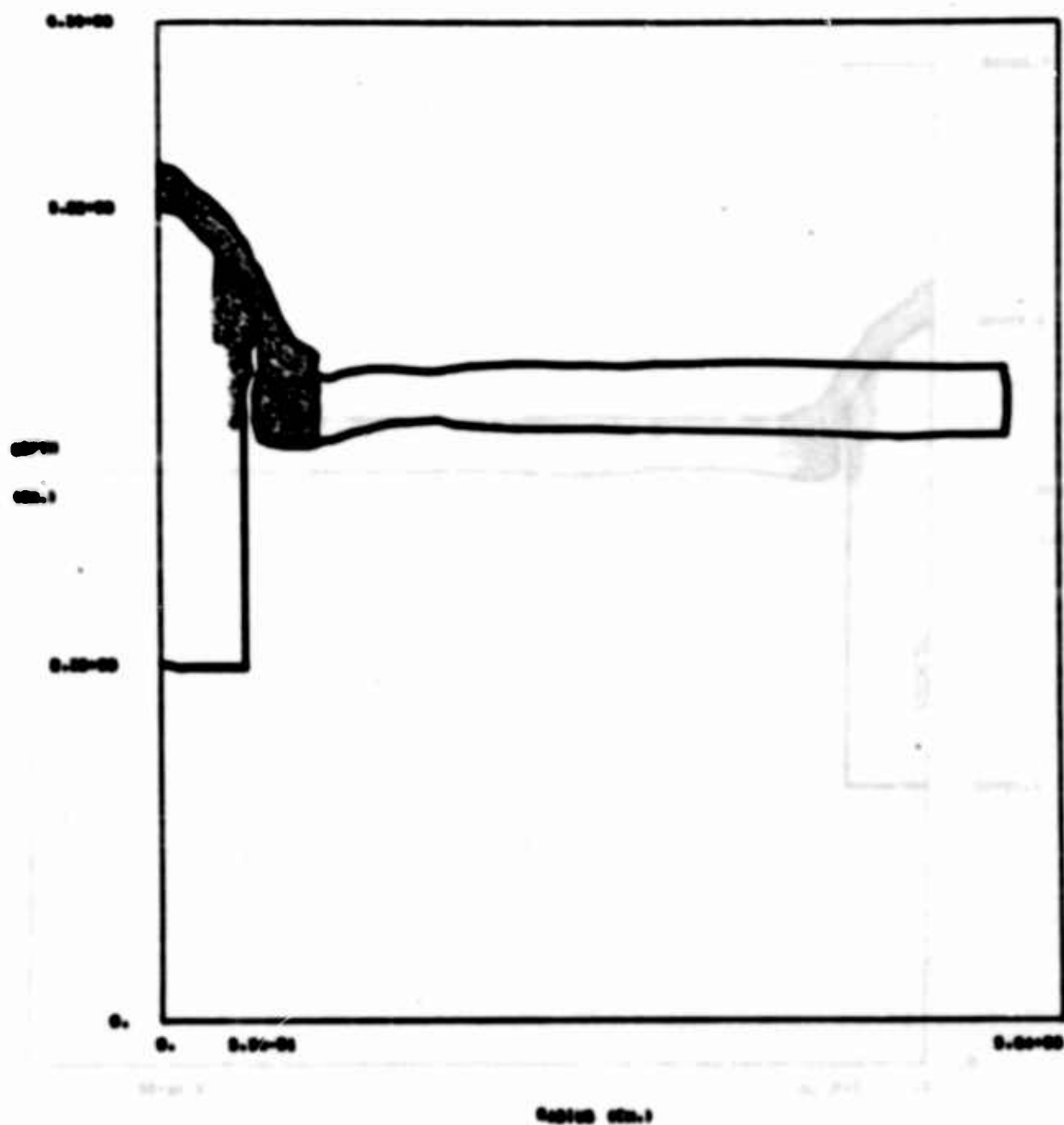


Fig. A.7--Russian projectile-target configuration
at $t = 20 \mu\text{sec}$.



**Fig. A.8--Russian projectile-target configuration
at $t = 30 \mu\text{sec}$.**

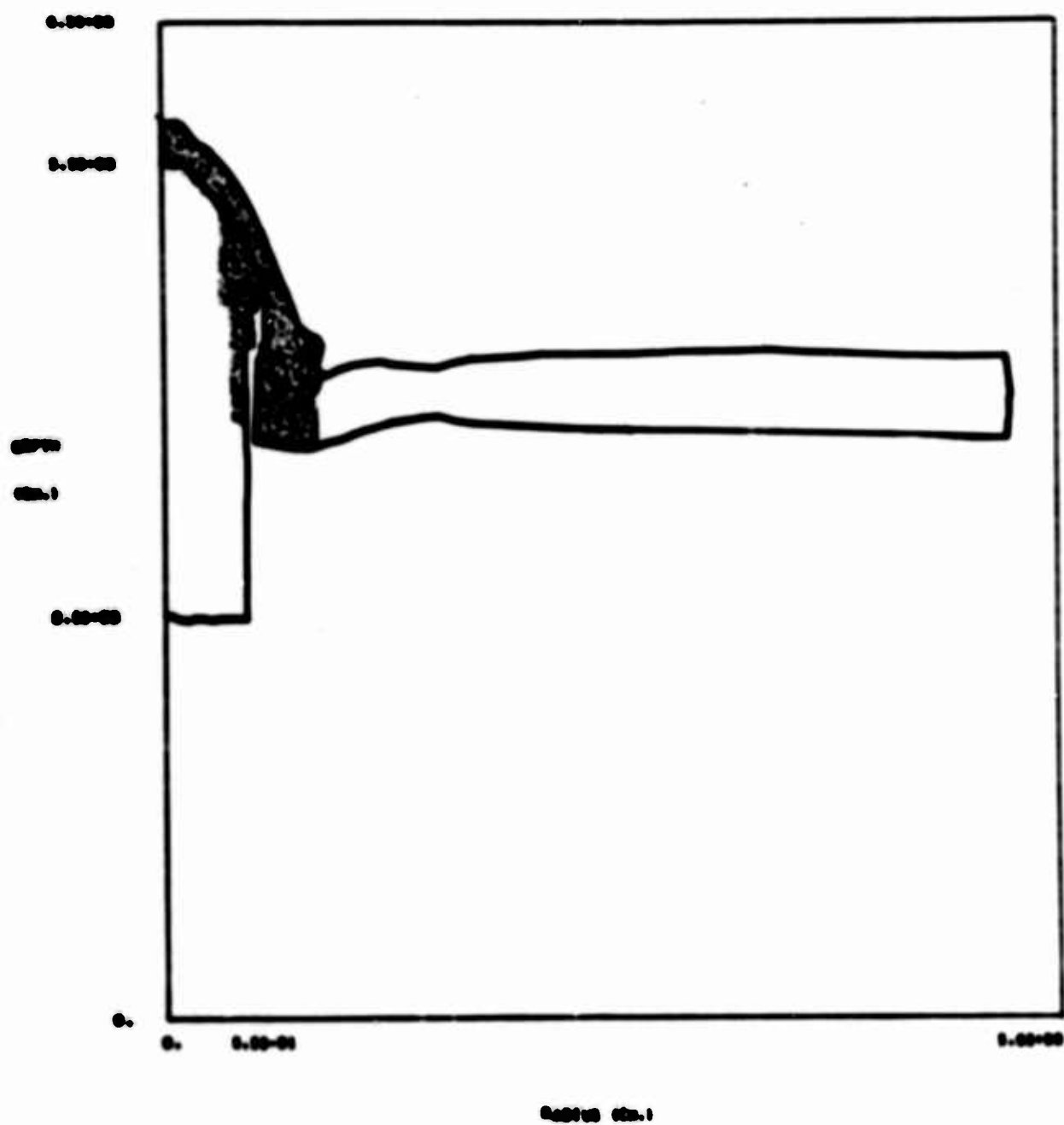


Fig. A.9--Russian projectile-target configuration
at $t = 36 \mu\text{sec}$.